

Sources of volcanic detritus in the basal Chinle Formation, southwestern Laurentia, and implications for the Early Mesozoic magmatic arc

N.R. Riggs¹, Z.A. Oberling^{1,*}, E.R. Howell^{1,†}, W.G. Parker², A.P. Barth³, M.R. Cecil⁴, and J.W. Martz⁵

¹School of Earth Sciences and Environmental Sustainability, Northern Arizona University, Flagstaff, Arizona 86011, USA

²Division of Resource Management, Petrified Forest National Park, Petrified Forest, Arizona 86028, USA

³Department of Earth Sciences, Indiana University–Purdue University Indianapolis, Indianapolis, Indiana 46202, USA

⁴Department of Geological Sciences, California State University Northridge, Northridge, California 91330, USA

⁵Department of Natural Sciences, University of Houston–Downtown, 1 Main Street, Houston, Texas 77002, USA

ABSTRACT

The Upper Triassic Chinle Formation in southwestern Laurentia is the oldest distinctive record of Early Mesozoic Cordilleran arc magmatism, in the form of detrital zircons and volcanic clasts. Initial deposition of the basal Shinarump and Mesa Redondo members, herein collectively called the Shinarump conglomerate, began in Late Triassic time, yet the earliest known arc magmatism is older by as much as 40 m.y.

Analysis of detrital zircons from eight sites in southeastern Nevada, southern Utah, and northeastern Arizona and volcanic-clast zircons from four of these sites provides a basis for understanding the evolution of the Early Mesozoic arc. Most Permian and Triassic detrital zircons from the Shinarump conglomerate have ages from ca. 260 to 220 Ma with rare grains as old as 280 Ma. These ages are compatible with derivation from sources in the magmatic arc to the west and southwest, including plutons of corresponding age in the Mojave Desert. Volcanic clasts are uniformly in the range 232–224 Ma; their age and zircon geochemistry argue against a source in currently exposed Mojave Desert Triassic plutons.

As a further test, we compared Th/U ratios of clast and detrital zircons with those of possible sources to the west. Th/U values of many detrital grains support their derivation from Triassic Mojave Desert plutons. Some detrital grains and those from the clasts, however, have Th/U values that are uniformly higher than those in Permo-Triassic Mojave Desert plutons and therefore argue for a different, unexposed source.

We propose that the early arc lay offshore of western Laurentia. Over time, plutons were emplaced across a range of continental crustal thicknesses that likely increased toward the east. At approximately 235–230 Ma, a land connection between the arc and retro-arc areas was established and fluvial sedi-

mentation began. The observation that the youngest grain ages in our detrital samples are variable suggests that this land connection was tenuous for perhaps 10 m.y. until well into Chinle Formation sedimentation.

INTRODUCTION

The inception of the Early Mesozoic Cordilleran magmatic arc along western Laurentia is recorded by plutons in the Mojave Desert and Sierra Nevada of California, United States (Barth and Wooden, 2006), and in Sonora, Mexico (Arvizu et al., 2009; Riggs et al., 2010), and by rare forearc and intra-arc sedimentary successions in Sonora (González-León, 1997; González-León et al., 2005) and the Mojave Desert (Carr et al., 1997; Stevens et al., 2005; Rains et al., 2012). One of the compelling enigmas of the earliest (i.e., Permian–Early Triassic) stage of arc evolution is the lack of a coeval retro-arc sedimentary record. Lower–Middle Permian sedimentary units exposed in eastern California through western and southern Arizona to central Sonora are part of the miogeoclinal margin that was truncated in late Paleozoic time (Walker, 1988; Stone and Stevens, 1988; Bateman, 1992; Miller et al., 1992; Saleeby et al., 1992; Dickinson and Lawton, 2001). Detrital zircons in the Lower–Middle Triassic Moenkopi Formation are considered to record magmatism to the southeast, consistent with paleocurrents from that direction (Dickinson and Gehrels, 2008). Analysis of the oldest unit that carries a widespread, unmistakable record of the arc, therefore, is necessary to understand its evolving tectonic setting and evolution of the Late Triassic landscape as arc magmatism became dominant along the southwest margin of Laurentia.

The Upper Triassic Chinle Formation (Fig. 1) was deposited in a broad basin behind the early Cordilleran arc beginning at ca. 230 Ma (Lawton, 1994; Dickinson and Gehrels, 2008). The basal Chinle Formation, which comprises the fluvial Shinarump and Mesa Redondo members, records the earliest distinctive influx of arc-related detritus in the form of detrital minerals and volcanic clasts.

*Present address: Call and Nicholas, Inc., 2475 N. Coyote Dr., Tucson, Arizona 85745, USA

†Present address: Noble Energy, 1625 Broadway, Suite 2200, Denver, Colorado 80202, USA

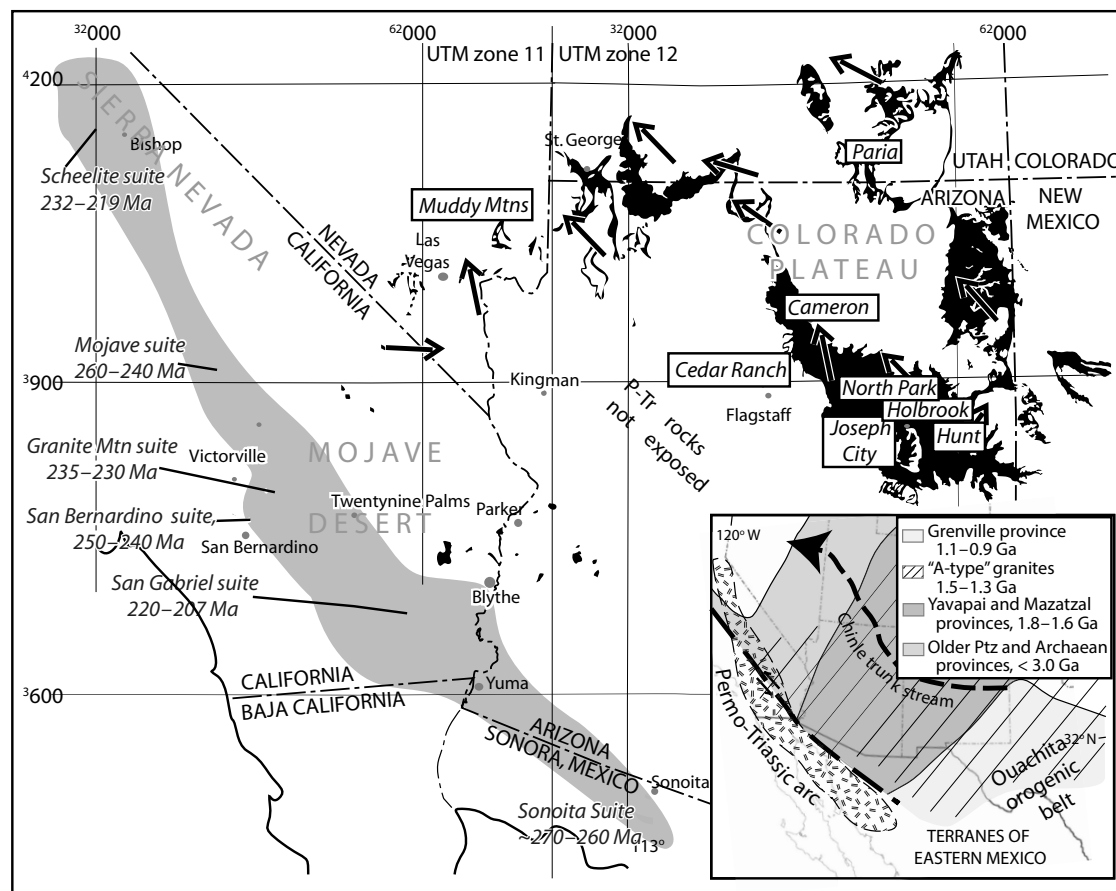


Figure 1. Map of Chinle Formation exposures (black) and Early Mesozoic magmatic arc (gray); arrows are paleocurrent directions (after Stewart et al., 1972b; Basdekas, 1993). Labels in boxes indicate Chinle sample sites. Inset map shows Proterozoic crustal provinces of southwestern Laurentia (after Wooden et al., 2012; Whitmeyer and Karlstrom, 2007). Coordinates are in Universal Transverse Mercator (UTM; NAD83 datum). P-Tr—Permo-Triassic; Ptz—Proterozoic.

We report here on a detailed detrital- and volcanic-zircon study of these basal fluvial sandstones and the volcanic clasts within them. Although paleocurrent directions (Stewart et al., 1972a) in general indicate that the Shinarump river systems flowed from southeast to northwest, a distinct Triassic detrital zircon signature together with the presence of Triassic volcanic clasts and local northeast flow directions record a significant contribution from the Cordilleran magmatic arc. We propose that the initial ~35–40 m.y. of arc magmatism occurred in an offshore arc, broadly analogous to the evolving Ryukyu arc-trench system, where the Philippine Sea is subducting under the Eurasian continental plate. As subduction became established and arc crust evolved and thickened by intra-arc contractional deformation and magmatism, the arc and retro-arc rose above sea level, providing a fluvial pathway for the deposition of arc-derived detritus into the Chinle basin. The dominant direction of flow and sedi-

ment flux, however, remained from the higher-elevation landmass to the east. Our purpose, therefore, is to document the diversity within the basal Chinle Formation and to propose how arc magmatism along the margin is reflected in these retro-arc sedimentary rocks.

TECTONIC SETTING

The Cordilleran magmatic arc developed across a truncated Paleozoic miogeoclinal margin along western Laurentia (Fig. 1) recorded by carbonate and siliciclastic passive-margin platform strata deposited on Precambrian basement. The early to mid-Paleozoic margin trended northeast-southwest, and Pennsylvanian–Permian sinistral strike-slip faulting created a northwest-south-

east-trending margin along which the Cordilleran arc formed (Walker, 1988; Stone and Stevens, 1988; Bateman, 1992; Miller et al., 1992; Saleeby et al., 1992; Dickinson and Lawton, 2001). The oldest plutonic rocks and volcanic detritus that record arc magmatism are 270–260 Ma plutons in Sonora, Mexico (Arvizu et al., 2009; Riggs et al., 2010), and ca. 280–265 Ma volcanic cobbles in forearc sedimentary strata (Riggs et al., 2010; Lindner et al., 2012). Likewise, Miller et al. (1995) and Barth and Wooden (2006) documented Permian–Middle Triassic plutonism (260–235 Ma) in the Mojave Desert of California. Related volcanic sections are exposed in the El Paso Mountains region of southeastern California, where andesite has been dated at ca. 260 Ma (Martin and Walker, 1995), and in the east-central Sierra Nevada, where successions are generally younger (ca. 230–215 Ma; Barth et al., 2011) than the oldest arc rocks in the southern Mojave Desert and Sonora.

Concurrently with the major change in tectonic activity along western Laurentia, the late Paleozoic Ouachita orogen along southeastern Laurentia (Fig. 1) created highlands that were the source of detritus moving from southeast to northwest across southern Laurentia. The Lower–Middle Triassic Moenkopi Formation contains this detritus (Dickinson and Gehrels, 2008). Dickinson and Gehrels (2008) suggested that the western facies of the Moenkopi Formation were deposited in a flexural foreland related to the Permo-Triassic Sonoma orogen. Facies indicate a marine (Stewart et al., 1972b) or tidal-zone (Reif and Slatt, 1979) environment of deposition in the westernmost deposits of the Moenkopi Formation.

■ CHINLE FORMATION

Deposition of the Chinle Formation resulted from dynamic subsidence related to development of the Cordilleran magmatic arc (Lawton, 1994; Dickinson and Gehrels, 2008). The formation comprises several members that dominantly record diverse fluvial environments (Stewart et al., 1972a; Blakey and Gubitosa, 1983; Lupe and Silberling, 1985; Dubiel, 1991). The Late Triassic age of the unit is constrained by paleontologic data (Camp, 1930; Colbert and Gregory, 1957; Fisher and Dunay, 1984; Lucas and Hunt, 1993) and by U-Pb dating of detrital zircons (LA-ICPMS: Riggs et al., 2003; Dickinson and Gehrels, 2008; ID-TIMS: Irmis et al., 2011; Ramezani et al., 2011, 2014; Atchley et al., 2013). In most exposures, the Chinle Formation was deposited on a significant erosional surface on the underlying Moenkopi Formation and represents a marked overall change in depositional environment from marine-tidal-sabkha to continental fluvial.

Shinarump and Mesa Redondo Members

The most precise date for the lower part of the Chinle Formation is provided by Atchley et al. (2013). Zircons from a tuffaceous sandstone near the base of the Mesa Redondo Member yielded a maximum depositional age of 227.604 ± 0.082 Ma. The Mesa Redondo and Shinarump members are likely lateral equivalents (see also supplementary data in Irmis et al., 2011), and thus

it is reasonable to infer that deposition of the Shinarump Member began no earlier than ca. 230 Ma (cf. Dickinson and Gehrels, 2008), as the sample dated by Atchley et al. (2013) does not come from the base of the formation.

The Shinarump Member comprises coarse to pebbly sandstone interbedded with conglomerate horizons. Clasts range from 1–2 cm to a maximum of 6–8 cm in diameter and are dominantly chert, quartzite, and limestone. Volcanic clasts are latitic, dacitic, and rhyolitic lava or tuff, are sparse, and make up a maximum of 5% of total clasts. Most clasts contain quartz, feldspars, and biotite (Table 1). Vitroclastic textures such as pumice and glass shards are common and indicate a pyroclastic origin, but evidence of welding is minor or lacking in the majority of clasts. A few clasts have euhedral phenocrysts and flow banding defined by devitrified glass and are interpreted as being derived from lava flow(s).

In general, volcanic clasts decrease in size and abundance from south to north, which has led to the speculation that the source of these clasts lay to the south in the “Mogollon Highlands” (Harshbarger et al., 1957; Stewart et al., 1972a; Dodge, 1973). Stewart et al. (1986) later noted that Mesozoic igneous rocks to the south of the Colorado Plateau are younger than Late Triassic and proposed that sources may have been faulted away from the area of southern Arizona, or lie hidden beneath younger cover. Reynolds et al. (1989) suggested that an unconformity between Proterozoic/Paleozoic rocks and Mesozoic sedimentary successions in western Arizona and eastern California records uplift that may have sourced detritus in the Chinle Formation, although those authors did not propose that this area was a source of volcanic material. More recently, Oberling et al. (2010) and Oberling (2015) have shown that volcanic clasts in the Shinarump Member show geochemical similarities to Triassic plutons in the Mojave Desert. Overall paleoflow was dominantly from the southeast (Stewart et al., 1972a; Blakey and Gubitosa, 1983), where highlands associated with the Ouachita orogen continued to contribute sediment. As discussed herein, however, the presence of volcanic clasts, Triassic detrital zircons, and local north-east-directed paleocurrents indicates that the Cordilleran volcanic arc was an additional and important source of detritus (e.g., Stewart et al., 1972b).

The Mesa Redondo Member is less well exposed than the Shinarump Member, overlying and interfingering with the Shinarump Member except where the Shinarump is not present (Cooley, 1958). In its type section and other regional exposures, the Mesa Redondo Member is dominantly siltstone and claystone with minor interstratified medium- to coarse-grained sandstone (Cooley, 1958; J.W. Martz and W.G. Parker, unpub. data). In many exposures of the Shinarump and Mesa Redondo members in northeastern Arizona, both units are capped by a well-developed plinthic oxisol (highly weathered deep soil horizon), locally referred to as the “mottled strata” (Stewart et al., 1972a; Dubiel and Hasiotis, 2011; Irmis et al., 2011) or “purple mottled unit” (Dubiel, 1987). This strongly suggests that these units are at least partially lateral equivalents (Irmis et al., 2011). Indeed, Akers (1964) did not distinguish the Shinarump and Mesa Redondo members in his geological map of eastern Arizona, and Therrien et al. (1999) interpreted the Shinarump and Mesa Redondo members together as channel and overbank deposits of the same fluvial system.

TABLE 1. MINERAL COMPOSITIONS AND VITROCLASTIC TEXTURES OF VOLCANIC CLASTS

Sample	Quartz (%)	Feldspar (%)	Biotite (%)	Fe-Ti oxide (%)	Pumice and/or glass shards	Degree of welding
Holbrook						
103009-1B*	20%	–	–	–	–	–
103009-1C*	1%	–	2%	–	–	–
103009-1D	15%	trace	1%	–	–	–
103009-1E*	15%	8%	1–2%	–	–	–
103009-1G*	10%	–	2%	–	X	Minor
103009-1H*	4–5%	–	–	–	–	–
103009-1I	2%	–	–	–	X	Moderate
103009-1J	10%	7%	1%	–	X	–
103009-1K*	18%	trace	–	trace	X	–
103009-1L	15%	7%	2–3%	–	–	–
052111-1A*	7%	8%	4%	–	X	Minor
052111-1B	15%	3%	2%	–	X	Minor
Cameron						
110609-1A	6%	–	–	1%	X	Minor
110609-1B*	12%	–	1%	–	–	–
110609-1C*	4–5%	–	–	–	X	Minor
110609-1D*	8–9%	–	–	–	X	Minor
110609-1E*	3%	4–5%	1%	–	X	Moderate
110609-1F*	4%	15%	2–3%	2%	X	–
110609-1H	10%	7%	–	1%	X	–
110609-2A	7%	–	–	1%	X	Moderate
110609-2B	5%	–	–	–	–	–
Joseph City						
JC-1	10%	10%	1%	1–2%	–	Moderate
JC-4	7%	4%	1%	–	X	Moderate
JCNEW-1A	13%	–	1–2%	trace	–	–
JCNEW-2A	10%	–	2%	10%	–	–
JCNEW-2B	7%	4%	2%	1–2%	–	–
JCNEW-2C	15%	1%	2%	2–3%	X	Minor
Hunt						
120309-1C	18%	–	1–2%	–	X	Minor
120309-1D	4–5%	–	2%	1%	–	–
120309-1E	–	–	1%	7%	X	Minor
120309-1F*	5%	1–2%	–	2%	X	Minor
120309-1G*	–	–	–	–	X	Minor
120309-1H*	12%	trace	trace	–	–	–
050511-1A	4%	–	1%	–	–	–
050511-2B	–	10%	3%	2%	–	–
050511-3A	4%	–	–	3%	X	–
050511-3B	10%	2%	3%	1%	X	–
050511-3C	–	–	–	–	X	–
050511-3D	8%	–	3–4%	–	X	Minor
050511-3E	4–5%	1–2%	1%	8%	X	–
050511-3F*	10%	–	3%	–	X	Minor
050511-3G	10%	3–4%	1%	trace	X	Moderate

Note: X indicates component present; – indicates component absent.

*Sampled yielded zircons (Tables 2A, 2B).

Sample Sites

Samples from eight locations, including those first discussed by Howell (2010), form the basis for this study. In total, samples were collected over an area of ~80,000 km², between ~150 km and ~450 km inboard of the Cordilleran arc (Muddy Mountains, Nevada, to Hunt, Arizona; Fig. 1). Post-Triassic deformation along the edge of the Colorado Plateau and in western Arizona–southern Nevada probably resulted in net extension between these sites and the arc. Precise correlation of clastic sedimentary units is impossible across these distances, and as discussed herein, the detrital zircon signature suggests that both the Shinarump and Mesa Redondo members make up the basal unit of the Chinle Formation. Therefore, we use the term “Shinarump conglomerate” to refer to the basal clastic unit that overlies redbeds and shallow-marine strata of the Lower–Middle Triassic Moenkopi Formation. In all cases, samples were collected from as close to the base of the Shinarump conglomerate as possible; the Hunt sample was collected stratigraphically a few meters above the sandstone dated by Atchley et al. (2013). All sample sites were traditionally assigned to the Shinarump Member except as noted. Tables 2A (analyses by LA-ICPMS) and 2B (analyses by SHRIMP-RG) provide analytical data for Shinarump conglomerate clasts; the Supplemental Table¹ has all analytical data for sandstone samples.

Muddy Mountains, Nevada (Universal Transverse Mercator [UTM] Zone 11, 0724396, 4033271; datum is NAD83 for all locations)

The Muddy Mountains, Nevada, site (Fig. 1; sample 111311-1, Supplemental Table) comprises coarse-grained sandstone interbedded with minor matrix- to clast-supported conglomerate lenses. Clasts are well rounded, poorly to moderately sorted, and granule- to cobble-sized chert and quartzite; no volcanic clasts were found at this site.

Detrital zircons from the Muddy Mountains are euhedral to rounded, with about equal parts rounded, euhedral, and subhedral grains. Euhedral grains are acicular to barrel shaped. In general, cathodoluminescence (CL) imagery shows that zoning bands within euhedral grains are parallel to grain boundaries and concentric through the entire grain, whereas those within rounded grains are rarely complete. In some euhedral grains, however, truncated zoning bands are overgrown by euhedral zoned rims.

Paria, Utah (UTM Zone 12, 0414669, 4121637)

The Paria, Utah, sample site (Fig. 1; sample 080310-1, Supplemental Table) exposes medium- to coarse-grained sandstone interbedded with minor matrix-supported conglomerate. Chert and quartzite clasts are typically well-rounded granules to pebbles; volcanic clasts are tan to white, angular, porphyritic fragments 1–3 cm in diameter that commonly occur in lenses. Volcanic clasts were not collected for analysis, however, due to their small size.

Detrital zircons from the Paria sample are dominantly subhedral to rounded, although rare grains are euhedral. Zoning bands are commonly truncated at grain boundaries. Euhedral and subhedral grains are barrel shaped to acicular.

Cedar Ranch, Arizona (UTM Zone 12, 0431976, 3933013; NAD 27)

The Cedar Ranch, Arizona, site (Fig. 1; sample 120310-2, Supplemental Table) is a small exposure on the northern margin of the San Francisco volcanic field. Medium- to coarse-grained sandstone is interbedded with conglomerate that contains well-rounded clasts of limestone, quartzite, and chert as much as 5 cm in diameter. Volcanic clasts were not found in the conglomerate at the Cedar Ranch site.

Far more of the detrital zircon grains from the Cedar Ranch sample are broken or blocky than in other samples. Most grains are barrel shaped or rounded; very few are acicular. In general, barrel-shaped grains have complete zoning bands preserved.

Cameron, Arizona (UTM Zone 12; sandstone: 0458111, 3993186; clasts: 0462820, 3970700)

Howell (2010) interpreted sandstone near Cameron, Arizona, (Fig. 1; sample Cameron, Supplemental Table) as Mesa Redondo Member. The sampled bed comprises large-scale trough cross-stratified, resistant but slope-forming medium-grained arkosic arenite with localized pebbles of chert and felsic volcanic material; the latter make up 2%–3% of clasts.

Clasts (sample 110609, Tables 2A, 2B) were collected from a moderately indurated, medium- to coarse-grained sandstone with conglomerate interbeds; this site is traditionally assigned to the Shinarump Member (Stewart et al., 1972a). The clasts range in size from pebble to cobble and are well rounded with poor to moderate sorting. The clast compositions range from quartzite, chert, and limestone to silicified and/or sericitized, porphyritic, rhyolitic tuff and lava; maximum clast size is 5–6 cm. CL imagery was obtained only on zircons from one clast; zoning bands in general parallel grain margins.

Holbrook, Arizona (UTM Zone 12, 0574867, 3863767)

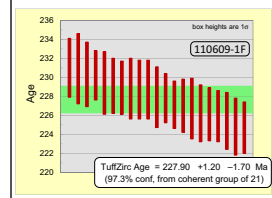
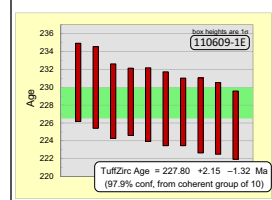
The Holbrook, Arizona, site (Fig. 1; sample 052111, Supplemental Table; samples 103009, 052111, Table 2A) has the highest percentage of volcanic clasts of any of the Shinarump conglomerate exposures. The section comprises medium- to coarse-grained sandstone with conglomerate interbeds that contain clast- to matrix-supported, well-rounded, poorly sorted granules to cobbles. Petrified wood is common. Clasts are dominantly quartzite, chert, and limestone; volcanic clasts are ~5% of all clasts. Maximum clast size overall is 5–6 cm.

¹Supplemental Table. LA-ICPMS analyses of detrital zircons from the Shinarump conglomerate. Please visit <http://dx.doi.org/10.1130/GES01238.S1> or the full-text article on www.gsapubs.org to view the Supplemental Table.

TABLE 2A. LA-ICPMS U-Pb ZIRCON DATA FOR SHINARUMP CONGLOMERATE CLASTS

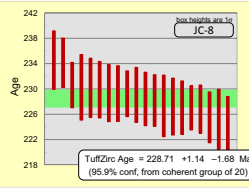
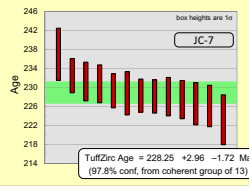
For the full-sized version of Table 2A, please visit <http://dx.doi.org/10.1130/GES01238.S2> or the full-text article on www.gsapubs.org.

Sample location and number	Measured isotopic ratios		Isotopic ages ^b										Concordance Filter	Best age (Ma)	error	Th/U	Clast age	Average clast Th/U				
			²⁰⁷ Pb/ ²³⁵ U		Error Correlation		Error Correlation		Age (Ma)		Age (Ma)								Age (Ma)			
U ppm ^a	Th ppm ^a	²⁰⁷ Pb/ ²³⁵ U	% error	²⁰⁶ Pb/ ²³⁸ U	% error	6/38-7/35	²⁰⁷ Pb/ ²⁰⁶ Pb	% error	38/6-7/6	²⁰⁷ Pb*/ ²⁰⁶ Pb*	error	²⁰⁶ Pb*/ ²³⁸ U	error	²⁰⁷ Pb*/ ²³⁵ U	error							
Cameron																						
110609-1C-1	255.728	489.844	0.2540	0.0052	0.0362	0.0006	0.7609	0.0512	0.0007	0.0151	249.8	55.5	228.9	3.7	230.0	4.3	1.00	229	4	1.924	Median age 231 Ma	1.34
110609-1C-2	164.794	193.449	0.2518	0.0064	0.0364	0.0006	0.6833	0.0507	0.0009	-0.0080	225.1	62.9	230.7	4.0	227.7	5.2	1.01	231	4	1.169		
110609-1C-4	124.462	114.637	0.2742	0.0074	0.0367	0.0006	0.6090	0.0541	0.0011	-0.0225	374.8	63.4	232.0	4.0	245.6	5.9	0.94	232	4	0.925		
110609-1C-3	326.967	209.043	0.2850	0.0062	0.0402	0.0008	0.8256	0.0511	0.0006	0.0974	246.3	52.5	253.8	4.8	254.8	4.8	1.00	254	5	0.632		
110609-1E-8	216.038	142.063	0.2495	0.0058	0.0356	0.0006	0.8021	0.0507	0.0007	-0.1187	225.0	57.0	225.7	3.8	225.9	4.7	1.00	226	4	0.657	228 ± 2 Ma	1.29
110609-1E-7	135.799	115.442	0.2543	0.0066	0.0358	0.0006	0.6155	0.0516	0.0010	0.0505	268.9	64.5	226.5	4.0	229.7	5.3	0.99	226	4	0.854		
110609-1E-9	98.599	129.908	0.2495	0.0076	0.0358	0.0007	0.6460	0.0506	0.0012	-0.0439	224.6	72.1	226.8	4.2	225.6	6.2	1.01	227	4	1.315		
110609-1E-2	295.005	242.824	0.2548	0.0051	0.0359	0.0006	0.8080	0.0517	0.0006	0.0586	272.5	53.2	227.2	3.8	230.7	4.0	0.98	227	4	0.830		
110609-1E-4	212.624	254.566	0.2526	0.0069	0.0359	0.0007	0.8467	0.0511	0.0008	-0.2230	245.0	57.8	227.6	4.1	228.3	5.6	1.00	228	4	1.154		
110609-1E-10	150.706	133.121	0.2495	0.0073	0.0360	0.0007	0.6883	0.0508	0.0011	-0.0364	230.2	67.1	228.0	4.1	225.7	5.9	1.01	228	4	0.891		
110609-1E-3	190.245	203.605	0.2557	0.0060	0.0361	0.0006	0.7339	0.0518	0.0008	0.0266	278.4	58.8	228.4	3.8	230.9	4.8	0.99	228	4	1.074		
110609-1E-6	76.337	580.025	0.2705	0.0109	0.0361	0.0007	0.5448	0.0551	0.0019	-0.1441	415.3	89.6	228.4	4.2	242.0	8.7	0.94	228	4	3.611		
110609-1E-5	380.046	653.358	0.2536	0.0063	0.0363	0.0007	0.8819	0.0511	0.0006	-0.1913	245.2	53.2	230.0	4.6	229.2	5.1	1.00	230	5	1.713		
110609-1E-1	68.547	53.980	0.2622	0.0081	0.0364	0.0007	0.5865	0.0523	0.0013	0.0413	300.1	73.5	230.5	4.4	235.9	6.5	0.98	231	4	0.801		
110609-1F-13	110.400	104.700	0.2456	0.0063	0.0355	0.0004	0.6034	0.0502	0.0010	-0.1532	204.3	65.5	224.7	2.7	223.3	5	1.01	225	3	0.957	228 ± 2 Ma	1.06
110609-1F-5	211.600	311.900	0.2543	0.0044	0.0355	0.0005	0.6165	0.0528	0.0007	0.1419	321.9	53.3	224.8	3	230.4	3.6	0.98	225	3	1.479		
110609-1F-19	138.000	109.800	0.2490	0.0051	0.0356	0.0005	0.5890	0.0510	0.0008	0.1377	241.3	58.3	225.4	3	225.6	4.1	1.00	225	3	0.798		
110609-1F-10	114.400	144.300	0.2522	0.0052	0.0357	0.0004	0.3738	0.0517	0.0010	0.2423	272.2	63.8	225.9	2.7	228.2	4.2	0.99	226	3	1.276		
110609-1F-16	98.600	68.680	0.2534	0.0065	0.0356	0.0004	0.5628	0.0517	0.0011	-0.0677	272.2	0	226.1	2.8	229.6	5.2	0.98	226	3	0.695		
110609-1F-20	175.000	247.300	0.2596	0.0049	0.0357	0.0005	0.7381	0.0526	0.0007	-0.0680	309.8	54.7	226.2	3	234.7	3.9	0.96	226	3	1.416		
110609-1F-11	91.300	70.700	0.2544	0.0066	0.0358	0.0005	0.5490	0.0519	0.0011	-0.0196	281.0	66.7	226.7	3.2	229.9	5.4	0.99	227	3	0.781		
110609-1F-3	92.000	104.800	0.2585	0.0053	0.0358	0.0005	0.4574	0.0531	0.0010	0.1522	332.6	61.7	227	2.8	233.3	4.3	0.97	227	3	1.146		
110609-1F-18	111.700	74.300	0.2532	0.0057	0.0359	0.0004	0.3942	0.0520	0.0011	0.1565	285.4	66.6	227.1	2.5	229.5	4.7	0.99	227	3	0.664		
110609-1F-8	105.400	115.900	0.2507	0.0053	0.0360	0.0004	0.4368	0.0511	0.0010	0.1209	244.0	64.2	227.8	2.6	227	4.3	1.00	228	3	1.110		
110609-1F-15	76.000	63.700	0.2542	0.0066	0.0360	0.0005	0.4476	0.0522	0.0012	0.1246	294.2	69.6	227.9	3.2	229.7	5.4	0.99	228	3	0.847		
110609-1F-6	52.580	41.090	0.2543	0.0072	0.0361	0.0005	0.5625	0.0516	0.0012	-0.0981	267.7	70.4	228.7	3.1	229.7	5.8	1.00	229	3	0.776		
110609-1F-12	282.100	541.200	0.2635	0.0045	0.0361	0.0005	0.7932	0.0533	0.0006	-0.0425	339.5	51.6	228.7	3.1	237.4	3.6	0.96	229	3	1.933		
110609-1F-1	104.800	176.000	0.2505	0.0055	0.0361	0.0005	0.4634	0.0507	0.0010	0.1777	227.2	64.9	228.8	3.2	227.3	4.5	1.01	229	3	1.631		
110609-1F-4	183.900	231.800	0.2492	0.0044	0.0362	0.0005	0.2953	0.0506	0.0008	0.3575	222.6	59.0	228.9	2.8	225.8	3.6	1.01	229	3	1.271		
110609-1F-21	188.400	201.100	0.2550	0.0045	0.0362	0.0005	0.6394	0.0512	0.0007	0.0917	249.4	55.8	229.1	2.9	231.4	3.6	0.99	229	3	1.072		
110609-1F-7	71.300	51.950	0.2594	0.0078	0.0362	0.0005	0.4800	0.0524	0.0013	0.0734	302.9	72.6	229.4	3.3	233.8	6.2	0.98	229	3	0.734		
110609-1F-24	179.200	176.200	0.2543	0.0045	0.0364	0.0004	0.6653	0.0508	0.0007	-0.1189	229.5	56.4	230.2	2.6	229.9	3.6	1.00	230	3	0.988		
110609-1F-23	61.300	60.600	0.2551	0.0071	0.0364	0.0006	0.3614	0.0502	0.0014	0.1048	204.3	79.6	230.3	3.4	230.4	5.7	1.00	230	3	0.978		
110609-1F-17	76.200	70.500	0.2534	0.0059	0.0365	0.0006	0.5283	0.0509	0.0010	0.1043	237.2	64.3	230.9	3.7	229.7	4.7	1.01	231	4	0.932		
110609-1F-2	81.300	58.500	0.2523	0.0063	0.0365	0.0005	0.4312	0.0504	0.0012	0.0817	213.5	72.0	231	3.1	228.2	5.1	1.01	231	3	0.726		
110609-1F-22	323.900	154.700	3.0660	0.0380	0.2462	0.0029	0.9710	0.0902	0.0003	0.0782	1428.9	0	1418	15	1424.3	9.2	0.99	1429	0	0.481		
110609-1F-9	23.960	16.630	0.3220	0.0330	0.0376	0.0008	0.5569	0.0609	0.0051	-0.3275	635.7	185.3	237.9	5	273	21	0.87	discordant	185	0.689		
110609-1F-14	136.500	193.400	0.4630	0.0390	0.0372	0.0006	0.6221	0.0896	0.0068	-0.4740	1417.0	150.1	235.1	3.7	378	27	0.17	discordant	150	1.433		



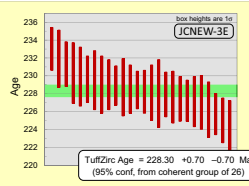
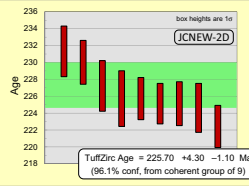
(continued)

TABLE 2A. LA-ICPMS U-Pb ZIRCON DATA FOR SHINARUMP CONGLOMERATE CLASTS (continued)

Sample location and number	Measured isotopic ratios		Isotopic ages ^b										Concordance Filter	Best age (Ma)	error	Th/U	Clast age	Average clast Th/U					
	U ppm ^a	Th ppm ^a	²⁰⁷ Pb/ ²³⁵ U	% error	²⁰⁶ Pb/ ²³⁸ U	% error	Error Correlation 6/38–7/35	²⁰⁷ Pb/ ²⁰⁶ Pb	% error	Error Correlation 38/6–7/6	Age (Ma)	error							Age (Ma)	error	Age (Ma)	error	
Joseph City																							
JC-8-19	208.513	335.778	0.2572	0.0064	0.0354	0.0007	0.7652	0.0528	0.0008	-0.0208	320.5	58.0	224.5	4.3	232.1	5.2	0.97	224	4	1.630	229 ± 2 Ma	1.12	
JC-8-15	54.598	78.133	0.2620	0.0085	0.0356	0.0008	0.4392	0.0534	0.0015	0.2293	346.7	76.8	225.2	4.8	235.7	6.8	0.96	225	5	1.458			
JC-8-12	255.720	297.072	0.2528	0.0059	0.0356	0.0006	0.8086	0.0509	0.0008	0.0168	234.4	58.0	225.5	4.0	228.6	4.8	0.99	225	4	1.185			
JC-8-5	327.964	596.336	0.2491	0.0053	0.0358	0.0006	0.8170	0.0505	0.0006	0.0222	216.7	53.6	226.8	3.8	225.6	4.3	1.01	227	4	1.862			
JC-8-23	169.441	135.290	0.2550	0.0055	0.0358	0.0006	0.6099	0.0510	0.0008	0.1854	242.6	58.5	227.0	3.5	231.3	4.4	0.98	227	3	0.809			
JC-8-18	117.600	117.889	0.2537	0.0067	0.0359	0.0007	0.6840	0.0514	0.0010	-0.0224	260.0	65.4	227.0	4.2	229.2	5.4	0.99	227	4	1.010			
JC-8-3	370.565	280.874	0.2565	0.0054	0.0359	0.0007	0.8587	0.0504	0.0005	0.1440	215.6	52.3	227.2	4.5	231.6	4.3	0.98	227	5	0.766			
JC-8-11	245.243	313.388	0.2503	0.0076	0.0359	0.0008	0.7914	0.0510	0.0010	-0.0909	239.4	64.3	227.3	4.9	226.4	6.2	1.00	227	5	1.269			
JC-8-16	187.034	236.257	0.2700	0.0105	0.0360	0.0007	0.6130	0.0535	0.0015	-0.2318	349.4	77.7	228.1	4.1	241.8	8.2	0.94	228	4	1.289			
JC-8-9	165.963	132.005	0.2497	0.0070	0.0361	0.0007	0.7467	0.0501	0.0009	-0.1011	199.1	61.8	228.4	4.2	226.5	5.6	1.01	228	4	0.805			
JC-8-8	152.527	94.406	0.2585	0.0070	0.0362	0.0007	0.6524	0.0517	0.0011	0.0771	270.7	65.4	229.0	4.4	233.7	5.7	0.98	229	4	0.616			
JC-8-21	109.288	90.256	0.2796	0.0091	0.0362	0.0006	0.4539	0.0563	0.0017	0.0630	463.9	78.6	229.2	3.6	249.6	7.2	0.92	229	4	0.843			
JC-8-6	68.674	120.493	0.2671	0.0091	0.0361	0.0007	0.5676	0.0533	0.0013	-0.0407	340.1	72.4	229.2	4.4	239.7	7.3	0.96	229	4	1.769			
JC-8-14	250.507	286.997	0.2489	0.0060	0.0362	0.0007	0.8262	0.0504	0.0007	0.0173	213.5	56.0	229.3	4.5	225.4	4.8	1.02	229	5	1.161			
JC-8-17	228.286	272.076	0.2680	0.0065	0.0363	0.0007	0.7836	0.0536	0.0008	0.0034	354.0	57.6	229.8	4.5	240.8	5.1	0.95	230	4	1.196			
JC-8-1	88.924	103.021	0.2753	0.0091	0.0364	0.0008	0.5527	0.0541	0.0016	0.0273	375.7	79.1	230.1	4.7	247.8	7.0	0.93	230	5	1.177			
JC-8-7	265.874	310.925	0.2525	0.0072	0.0364	0.0008	0.8333	0.0509	0.0008	0.0279	237.1	58.8	230.2	5.2	228.8	5.9	1.01	230	5	1.171			
JC-8-4	416.323	330.553	0.2545	0.0051	0.0364	0.0006	0.8284	0.0511	0.0006	-0.0960	246.7	54.0	230.6	3.6	230.0	4.1	1.00	231	4	0.807			
JC-8-2	225.800	177.711	0.2636	0.0061	0.0370	0.0006	0.7735	0.0515	0.0007	-0.0149	265.1	55.2	234.1	3.9	237.2	4.9	0.99	234	4	0.798			
JC-8-10	383.683	380.742	0.2561	0.0062	0.0371	0.0007	0.8412	0.0506	0.0007	-0.1004	223.7	55.1	234.5	4.6	231.8	4.9	1.01	235	5	0.854			
JC-8-13	213.096	141.758	3.0874	0.0640	0.2489	0.0050	0.9781	0.0899	0.0004	0.0622	1423.7	39.0	1431.3	25.9	1428.0	15.7	1.01	1424	39	0.651			
JC-8-20	320.355	10.338	3.0753	0.0483	0.2454	0.0038	0.9803	0.0907	0.0003	0.0398	1439.3	38.6	1414.1	19.4	1425.8	12.3	0.98	1439	39	0.029			
JC-8-22	187.731	142.949	0.2910	0.0142	0.0355	0.0005	0.4937	0.0603	0.0028	-0.2383	612.9	108.7	224.6	3.2	257.8	10.8	0.37	discordant	3	0.740			
JC-7-5	264.563	284.157	0.2456	0.0071	0.0352	0.0008	0.8589	0.0509	0.0007	-0.1133	236.1	57.3	223.2	5.3	223.2	5.9	1.00	223	5	1.069	228 ± 3 Ma	1.20	
JC-7-6	264.712	345.645	0.2556	0.0063	0.0357	0.0007	0.8213	0.0525	0.0007	-0.1099	306.9	55.3	226.1	4.4	230.8	5.1	0.98	226	4	1.294			
JC-7-1	84.597	98.024	0.2461	0.0086	0.0358	0.0007	0.6474	0.0506	0.0014	-0.0355	223.1	77.6	226.5	4.4	222.7	7.0	1.02	227	4	1.186			
JC-7-12	323.517	469.289	0.2540	0.0054	0.0359	0.0006	0.8087	0.0513	0.0007	0.0977	252.1	55.0	227.4	4.0	230.0	4.3	0.99	227	4	1.465			
JC-7-11	375.592	691.555	0.2513	0.0046	0.0360	0.0007	0.8819	0.0509	0.0005	0.2050	235.3	51.5	228.0	4.1	227.5	3.8	1.00	228	4	1.871			
JC-7-8	931.961	822.103	0.2562	0.0044	0.0360	0.0006	0.8748	0.0515	0.0004	0.0651	263.7	49.4	228.1	3.5	231.4	3.5	0.99	228	4	0.886			
JC-7-13	459.355	623.828	0.2538	0.0048	0.0360	0.0006	0.8044	0.0511	0.0006	0.1255	243.7	52.6	228.3	3.5	229.8	3.9	0.99	228	3	1.332			
JC-7-3	195.477	168.032	0.2576	0.0067	0.0361	0.0007	0.7926	0.0520	0.0008	-0.0302	287.1	58.7	228.7	4.6	232.8	5.5	0.98	229	5	0.863			
JC-7-10	427.030	492.272	0.2578	0.0047	0.0362	0.0006	0.8944	0.0513	0.0005	-0.0867	253.6	50.4	229.3	3.6	232.7	3.8	0.99	229	4	1.150			
JC-7-7	514.911	692.507	0.2646	0.0055	0.0364	0.0006	0.8833	0.0526	0.0006	0.1115	309.5	51.8	230.7	4.0	238.6	4.5	0.97	231	4	1.345			
JC-7-4	229.270	289.987	0.2671	0.0077	0.0365	0.0007	0.7052	0.0538	0.0011	-0.0864	363.6	63.5	231.2	4.1	239.9	6.1	0.96	231	4	1.155			
JC-7-9	129.755	104.302	0.2581	0.0062	0.0367	0.0006	0.6667	0.0518	0.0009	0.0876	276.0	61.7	232.5	3.6	233.8	4.8	0.99	232	4	0.790			
JC-7-2	537.259	651.784	0.2913	0.0085	0.0375	0.0009	0.8031	0.0569	0.0010	-0.0189	488.5	57.6	237.0	5.5	259.0	6.7	0.92	237	5	1.218			
JCNEW-2E-8	78.600	112.000	0.2551	0.0067	0.0354	0.0004	0.3314	0.0523	0.0014	0.0907	298.5	76.2	224	2.8	231.8	5.4	0.97	224	3	1.436	228 ± 2 Ma	1.08	
JCNEW-2E-23	106.200	117.100	0.2532	0.0056	0.0355	0.0004	0.4823	0.0513	0.0010	0.0336	254.3	64.2	225	2.5	229.5	4.6	0.98	225	3	1.109			
JCNEW-2E-7	128.100	118.800	0.2678	0.0053	0.0356	0.0004	0.4441	0.0537	0.0009	0.0591	357.2	60.0	226	2.3	240.7	4.2	0.94	226	2	0.932			
JCNEW-2E-27	134.300	184.000	0.2552	0.0052	0.0357	0.0005	0.6395	0.0517	0.0009	0.0955	273.5	59.3	226	3.1	230.6	4.2	0.98	226	3	1.360			
JCNEW-2E-20	91.200	106.600	0.2602	0.0066	0.0359	0.0005	0.4733	0.0528	0.0012	0.0719	320.2	68.8	227	3	234.6	5.3	0.97	227	3	1.171			
JCNEW-2E-2	95.500	77.600	0.2537	0.0049	0.0359	0.0005	0.5440	0.0511	0.0009	0.0885	245.8	61.7	227	2.8	229.4	4	0.99	227	3	0.829			
JCNEW-2E-1	70.800	50.810	0.2524	0.0061	0.0359	0.0004	0.3076	0.0509	0.0012	0.1857	236.3	71.3	227	2.3	228.8	4.9	0.99	227	2	0.712			

(continued)

TABLE 2A. LA-ICPMS U-Pb ZIRCON DATA FOR SHINARUMP CONGLOMERATE CLASTS (continued)

Sample location and number	Measured isotopic ratios		Isotopic ages ^b									Concordance Filter	Best age (Ma)	error	Th/U	Clast age	Average clast Th/U					
	U ppm ^a	Th ppm ^a	²⁰⁷ Pb/ ²³⁵ U	% error	²⁰⁶ Pb/ ²³⁸ U	% error	6/38–7/35	²⁰⁷ Pb/ ²⁰⁶ Pb	% error	38/6–7/6	Age (Ma)							error	Age (Ma)	error	Age (Ma)	error
Joseph City (continued)																						
JCNEW-2E-14	100.200	73.000	0.2516	0.0060	0.0359	0.0004	0.5121	0.0504	0.0010	-0.0050	215.3	64.6	227	2.5	228.2	4.9	1.00	227	3	0.728		
JCNEW-2E-29	70.200	101.200	0.2594	0.0072	0.0360	0.0005	0.3233	0.0520	0.0014	0.1675	285.4	76.7	228	2.9	234.6	5.7	0.97	228	3	1.442		
JCNEW-2E-24	159.700	235.000	0.2566	0.0045	0.0360	0.0004	0.6010	0.0513	0.0008	0.1310	253.9	57.2	228	2.5	232.2	3.6	0.98	228	3	1.414		
JCNEW-2E-25	48.720	59.600	0.2632	0.0089	0.0360	0.0006	0.4760	0.0531	0.0017	-0.0086	333.1	85.6	228	3.8	236.7	7.2	0.96	228	4	1.232		
JCNEW-2E-26	88.700	95.900	0.2568	0.0069	0.0360	0.0005	0.5015	0.0516	0.0011	0.0056	267.7	67.1	228	3.1	233	5.7	0.98	228	3	1.092		
JCNEW-2E-5	119.800	111.500	0.2576	0.0060	0.0360	0.0004	0.4765	0.0516	0.0011	0.0261	267.7	67.1	228	2.4	233.1	4.9	0.98	228	2	0.938		
JCNEW-2E-6	158.000	187.600	0.2605	0.0040	0.0361	0.0003	0.5887	0.0515	0.0007	-0.0360	262.4	54.8	228	2.1	234.9	3.2	0.97	228	2	1.186		
JCNEW-2E-10	162.300	197.200	0.2563	0.0056	0.0361	0.0004	0.5894	0.0514	0.0009	0.0078	259.7	61.1	229	2.7	231.5	4.5	0.99	229	3	1.220		
JCNEW-2E-30	115.600	98.400	0.2811	0.0099	0.0361	0.0005	0.4629	0.0559	0.0017	-0.0772	448.4	80.9	229	3.2	250.9	7.8	0.91	229	3	0.861		
JCNEW-2E-15	151.200	127.100	0.2504	0.0054	0.0362	0.0004	0.4561	0.0497	0.0009	0.0681	181.0	63.5	229	2.2	226.7	4.4	1.01	229	2	0.840		
JCNEW-2E-17	156.600	154.000	0.2508	0.0049	0.0362	0.0005	0.6430	0.0499	0.0008	0.0258	189.9	58.8	229	3.2	227	4	1.01	229	3	0.988		
JCNEW-2E-22	130.600	184.700	0.2559	0.0049	0.0362	0.0005	0.5657	0.0508	0.0008	0.0229	231.3	59.4	229	2.8	231.2	4	0.99	229	3	1.433		
JCNEW-2E-18	70.000	71.900	0.2712	0.0078	0.0362	0.0005	0.5113	0.0539	0.0013	-0.0064	366.9	70.6	230	3.3	243.3	6.2	0.94	230	3	1.042		
JCNEW-2E-12	164.900	177.500	0.2499	0.0048	0.0363	0.0004	0.6478	0.0499	0.0007	0.0120	189.9	57.9	230	2.6	226.3	3.9	1.01	230	3	1.084		
JCNEW-2E-28	78.900	110.600	0.2630	0.0075	0.0363	0.0005	0.4827	0.0513	0.0012	0.0671	254.3	70.8	230	3.3	236.7	6	0.97	230	3	1.413		
JCNEW-2E-13	139.300	117.800	0.2541	0.0059	0.0364	0.0005	0.5857	0.0504	0.0009	0.1110	211.2	60.7	230	3.4	229.7	4.7	1.00	230	3	0.846		
JCNEW-2E-4	97.750	93.100	0.2562	0.0053	0.0365	0.0004	0.5402	0.0510	0.0009	-0.0225	241.3	61.5	231	2.5	231.4	4.3	1.00	231	3	0.941		
JCNEW-2E-9	132.900	126.600	0.2638	0.0048	0.0366	0.0005	0.6132	0.0522	0.0008	0.1685	294.2	58.3	232	3.2	238.1	3.9	0.97	232	3	0.953		
JCNEW-2E-16	72.000	56.300	0.2654	0.0074	0.0368	0.0004	0.3042	0.0513	0.0014	0.0592	254.3	77.8	233	2.4	238.6	5.9	0.98	233	2	0.789		
JCNEW-2E-19	46.970	41.570	1.9260	0.0260	0.1837	0.0020	0.6857	0.0759	0.0008	0.2363	1093.5	45.0	1087	11	1089.2	8.9	0.99	1093	45	0.892		
JCNEW-2E-11	899.000	348.000	4.1180	0.0520	0.2943	0.0036	0.9924	0.1009	0.0002	-0.0295	1639.8	37.3	1662	18	1657	10	1.01	1640	37	0.389		
JCNEW-2E-3	66.500	62.600	0.3380	0.0350	0.0371	0.0006	0.7102	0.0649	0.0059	-0.5953	771.1	195.9	235	3.8	289	24	0.30	discordant	196	0.951		
JCNEW-2E-21	235.000	58.480	2.7900	0.0750	0.2147	0.0049	0.9812	0.0931	0.0006	-0.6198	1490.1	40.0	1253	26	1348	21	0.84	discordant	40	0.249		
225 ± 3 Ma																						
JCNEW-2D-1	98.900	149.500	0.2490	0.0062	0.0351	0.0004	0.5285	0.0517	0.0011	-0.1143	272.2	66.9	222.4	2.5	226.1	5.2	0.98	222	3	1.493		
JCNEW-2D-7	122.900	124.100	0.2502	0.0065	0.0355	0.0005	0.4800	0.0511	0.0010	-0.1814	245.3	64.4	224.6	2.9	226.5	5.3	0.99	225	3	1.015		
JCNEW-2D-6	422.500	758.000	0.2491	0.0039	0.0355	0.0004	0.8157	0.0508	0.0005	-0.1892	231.3	50.9	225.1	2.4	225.7	3.2	1.00	225	2	1.807		
JCNEW-2D-8	403.600	376.000	0.2489	0.0036	0.0355	0.0004	0.7213	0.0508	0.0005	0.1352	230.4	52.3	225.1	2.6	225.6	3	1.00	225	3	0.935		
JCNEW-2D-2	210.700	489.600	0.2493	0.0050	0.0356	0.0005	0.6565	0.0509	0.0008	0.0631	237.7	0.0	225.7	3.3	225.8	4.1	1.00	226	3	2.342		
JCNEW-2D-9	286.900	303.100	0.2506	0.0043	0.0356	0.0004	0.7010	0.0511	0.0006	-0.0467	243.5	53.4	225.7	2.5	226.9	3.5	0.99	226	3	1.067		
JCNEW-2D-10	546.100	545.900	0.2511	0.0039	0.0359	0.0005	0.8182	0.0507	0.0005	-0.0166	225.4	51.0	227.2	3	227.7	3.3	1.00	227	3	1.008		
JCNEW-2D-3	185.700	201.400	0.2531	0.0040	0.0363	0.0004	0.5312	0.0502	0.0007	0.2245	203.3	56.3	230	2.6	229	3.2	1.00	230	3	1.071		
JCNEW-2D-5	81.600	107.600	0.2636	0.0058	0.0365	0.0005	0.3724	0.0525	0.0012	0.1711	307.2	69.2	231.3	3	237.3	4.7	0.97	231	3	1.340		
JCNEW-2D-4	67.610	105.600	0.4120	0.0220	0.0380	0.0006	0.5163	0.0791	0.0037	-0.2420	1174.6	100.7	240.3	3.6	349	16	0.20	discordant	101	1.573		
Hunt																						
120309-1F-1	161.700	391.800	0.2469	0.0074	0.0351	0.0008	0.7267	0.0506	0.0010	0.0384	222.6	65.0	222.1	4.8	223.7	6	0.99	222	5	2.427	<p>Median age 224 Ma</p>	1.40
120309-1F-2	178.000	137.400	0.2518	0.0058	0.0353	0.0008	0.7036	0.0521	0.0009	0.2996	287.6	61.6	223.8	4.9	227.8	4.7	0.98	224	5	0.772		
120309-1F-5	18.800	31.500	0.2690	0.0190	0.0353	0.0014	0.0700	0.0559	0.0042	0.3863	448.4	172.7	223.8	8.9	240	15	0.93	224	9	1.681		
120309-1F-3	188.200	163.400	0.2562	0.0060	0.0358	0.0007	0.7917	0.0518	0.0008	0.0522	277.5	57.6	226.7	4.6	231.3	4.9	0.98	227	5	0.872		
120309-1F-4	35.520	44.200	0.2700	0.0120	0.0363	0.0008	0.5018	0.0540	0.0020	-0.0541	371.0	94.8	229.5	4.9	241.8	9.4	0.95	230	5	1.252		

(continued)

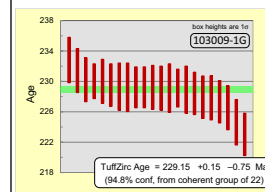
TABLE 2A. LA-ICPMS U-Pb ZIRCON DATA FOR SHINARUMP CONGLOMERATE CLASTS (continued)

Sample location and number	Measured isotopic ratios		Isotopic ages ^b								Concordance Filter	Best age (Ma)	error	Th/U	Clast age	Average clast Th/U							
	U ppm ^a	Th ppm ^a	²⁰⁷ Pb/ ²³⁵ U	% error	²⁰⁶ Pb/ ²³⁸ U	% error	6/38–7/35	Correlation	Correlation	Age (Ma)							error	Age (Ma)	error	Age (Ma)	error		
Hunt (continued)																							
120309-1H-6	99.211	102.092	0.2484	0.0076	0.0351	0.0007	0.6072	0.0511	0.0012	0.0140	244.1	72.5	222.2	4.4	224.8	6.1	0.99	222	4	1.037	229 +3/-5 Ma	1.37	
120309-1H-8	246.235	299.554	0.2467	0.0053	0.0353	0.0007	0.7944	0.0501	0.0007	0.1057	200.9	57.2	223.7	4.4	223.7	4.3	1.00	224	4	1.280			
120309-1H-1	387.188	407.275	0.2495	0.0049	0.0359	0.0007	0.8666	0.0506	0.0005	0.0258	224.6	52.4	227.3	4.2	226.0	4.0	1.01	227	4	0.971			
120309-1H-2	381.659	875.160	0.2577	0.0058	0.0360	0.0006	0.8225	0.0512	0.0006	-0.1090	248.6	53.9	227.7	3.8	232.5	4.7	0.98	228	4	2.243			
120309-1H-4	430.316	531.361	0.2534	0.0047	0.0363	0.0006	0.8119	0.0504	0.0005	0.0561	212.8	52.4	229.7	3.6	229.2	3.8	1.00	230	4	1.245			
120309-1H-3	372.384	435.379	0.2533	0.0057	0.0365	0.0006	0.8750	0.0503	0.0005	-0.1778	208.6	52.8	230.8	3.7	229.0	4.6	1.01	231	4	1.173			
120309-1H-5	207.720	309.045	0.2589	0.0064	0.0365	0.0006	0.7051	0.0515	0.0009	-0.0651	263.3	60.6	231.3	3.8	233.5	5.1	0.99	231	4	1.364			
120309-1H-7	219.409	351.881	0.2713	0.0078	0.0372	0.0008	0.7351	0.0527	0.0009	-0.1256	316.5	60.7	235.2	4.9	243.2	6.2	0.97	235	5	1.622			
120309-1G-17	121.300	100.600	0.2614	0.0061	0.0357	0.0004	0.5258	0.0531	0.0011	-0.0104	333.1	65.3	226.2	2.6	236.2	4.8	0.96	226	3	1.213	229 ± 3 Ma	0.81	
120309-1G-20	627.700	1092.000	0.2511	0.0042	0.0358	0.0005	0.9127	0.0511	0.0004	0.2720	243.1	49.8	227	3.2	227.3	3.4	1.00	227	3	0.576			
120309-1G-11	66.780	84.890	0.2561	0.0075	0.0360	0.0004	0.3635	0.0520	0.0015	0.0587	285.4	80.3	228.1	2.8	231.2	6.1	0.99	228	3	0.778			
120309-1G-5	53.220	54.550	0.2794	0.0079	0.0364	0.0005	0.3938	0.0560	0.0016	0.0178	452.4	77.4	230.2	3.2	249.8	6.2	0.92	230	3	0.980			
120309-1G-14	183.000	281.600	0.2528	0.0048	0.0364	0.0005	0.7404	0.0506	0.0006	-0.0125	220.8	54.3	230.7	3.1	229.6	3.9	1.00	231	3	0.657			
120309-1G-13	202.500	315.100	0.2587	0.0044	0.0366	0.0004	0.6560	0.0519	0.0007	0.0237	279.7	55.7	231.9	2.5	233.5	3.5	0.99	232	3	0.639			
120309-1G-9	376.100	247.000	0.2865	0.0037	0.0407	0.0005	0.7901	0.0516	0.0004	0.1163	269.1	49.5	257	2.8	255.7	2.9	1.01	257	3	1.520			
120309-1G-3	97.900	75.900	0.2981	0.0064	0.0414	0.0006	0.5564	0.0522	0.0008	0.0722	295.1	58.6	261.2	3.4	264.6	5	0.99	261	3	1.285			
120309-1G-1	239.700	103.500	0.3247	0.0060	0.0453	0.0007	0.7323	0.0527	0.0006	0.0293	315.9	52.8	285.8	4	285.3	4.6	1.00	286	4	2.321			
120309-1G-6	368.100	93.300	0.3287	0.0056	0.0457	0.0006	0.8029	0.0524	0.0005	0.0460	304.6	50.3	288.1	3.8	288.4	4.3	1.00	288	4	3.962			
120309-1G-16	71.000	54.400	0.7500	0.0160	0.0905	0.0012	0.7257	0.0607	0.0009	-0.1247	628.6	53.4	558.6	6.9	568.5	9	0.98	559	7	1.305			
120309-1G-4	173.100	81.800	3.1700	0.0470	0.2553	0.0035	0.9599	0.0910	0.0004	-0.1037	1446.0	38.9	1465	18	1450	11	1.01	1446	39	2.129			
120309-1G-15	79.300	89.350	3.1610	0.0490	0.2544	0.0037	0.9170	0.0913	0.0006	0.0790	1452.2	39.7	1460	19	1446	12	1.01	1452	40	0.889			
120309-1G-12	676.000	208.700	2.9490	0.0380	0.2365	0.0031	0.9797	0.0916	0.0003	-0.0711	1459.9	38.4	1368	16	1393.6	9.9	0.94	1460	38	3.208			
120309-1G-19	420.500	931.000	3.1800	0.0330	0.2531	0.0025	0.9718	0.0917	0.0002	0.0743	1460.1	38.3	1454	13	1451.6	8	1.00	1460	38	0.464			
120309-1G-7	396.100	341.400	3.1320	0.0370	0.2474	0.0033	0.9446	0.0927	0.0004	0.3831	1481.4	38.7	1425	17	1439.7	9.1	0.96	1481	39	1.163			
120309-1G-18	762.000	71.700	3.5470	0.0520	0.2659	0.0038	0.9907	0.0979	0.0002	-0.1345	1583.5	37.7	1519	19	1538	12	0.96	1584	38	10.530			
120309-1G-2	104.900	120.200	3.5500	0.0530	0.2576	0.0036	0.7005	0.1012	0.0011	0.0274	1646.2	42.2	1477	18	1537	12	0.90	1646	42	0.870			
120309-1G-10	31.300	17.430	4.0050	0.0730	0.2879	0.0041	0.8328	0.1017	0.0011	-0.0062	1655.4	42.1	1630	20	1633	15	0.98	1655	42	1.806			
120309-1G-21	130.000	107.000	7.0660	0.0820	0.3883	0.0043	0.9658	0.1325	0.0004	0.0984	2131.9	35.4	2114	20	2120	11	0.99	2132	35	1.212			
120309-1G-8	155.000	118.900	0.3010	0.0110	0.0364	0.0004	0.4230	0.0610	0.0021	-0.1538	639.2	85.6	230.4	2.6	266.5	8.5	0.36	discordant	86	1.304			
050511-2C-2	174.900	232.000	0.2455	0.0040	0.0350	0.0004	0.6028	0.0499	0.0008	0.0873	192.2	58.2	222	2.7	222.8	3.2	1.00	222	3	0.753	Median age 223 Ma	0.75	
050511-2C-1	128.100	221.300	0.2506	0.0043	0.0351	0.0004	0.5696	0.0514	0.0008	0.0945	256.6	57.5	222.4	2.5	226.9	3.5	0.98	222	3	0.579			
050511-2C-3	179.500	196.100	0.2604	0.0068	0.0354	0.0005	0.5173	0.0529	0.0010	-0.1621	322.8	61.7	224	3.2	234.7	5.4	0.95	224	3	0.912			
050511-2C-4	74.300	99.800	0.2594	0.0071	0.0357	0.0005	0.3263	0.0524	0.0014	0.1752	302.9	76.1	226.1	3.2	233.9	5.7	0.97	226	3	0.745			
050511-3F-4	419.400	574.800	0.2458	0.0037	0.0353	0.0005	0.7587	0.0506	0.0005	0.1158	223.1	51.6	223.5	2.8	223.5	3	1.00	224	3	0.731	230 +6/-2 Ma	0.66	
050511-3F-7	165.400	347.300	0.2551	0.0054	0.0358	0.0005	0.7082	0.0513	0.0008	-0.0491	252.5	58.1	227	3.2	231.1	4.3	0.98	227	3	0.475			
050511-3F-9	104.400	193.800	0.2626	0.0063	0.0359	0.0005	0.4070	0.0536	0.0011	0.1200	354.3	64.7	227.3	2.9	236.5	5.1	0.96	227	3	0.538			
050511-3F-2	538.800	499.400	0.2534	0.0037	0.0360	0.0004	0.8084	0.0509	0.0004	0.1034	238.1	50.1	227.7	2.7	229.6	3	0.99	228	3	1.079			
050511-3F-8	155.900	164.900	0.2539	0.0050	0.0360	0.0005	0.6957	0.0514	0.0008	-0.0694	259.3	57.4	228.1	3	230.1	4.1	0.99	228	3	0.942			
050511-3F-11	86.630	157.500	0.2554	0.0073	0.0360	0.0006	0.6157	0.0516	0.0011	-0.1118	267.7	67.1	228.1	3.5	232.1	6.1	0.98	228	4	0.544			
050511-3F-5	90.000	181.100	0.2544	0.0063	0.0362	0.0004	0.2102	0.0505	0.0013	0.2418	218.1	75.5	229	2.7	229.9	5.1	1.00	229	3	0.498			
050511-3F-1	118.200	247.000	0.2544	0.0063	0.0362	0.0005	0.6784	0.0509	0.0010	-0.1832	234.5	63.2	229.4	3	229.8	5.1	1.00	229	3	0.476			

(continued)

TABLE 2A. LA-ICPMS U-Pb ZIRCON DATA FOR SHINARUMP CONGLOMERATE CLASTS (continued)

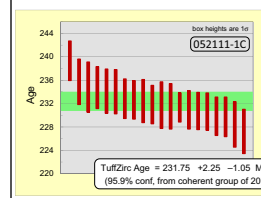
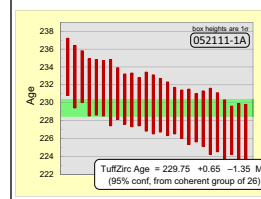
Sample location and number	U ppm ^a		Measured isotopic ratios							Isotopic ages ^b						Concordance Filter	Best age (Ma)	error	Th/U	Clast age	Average clast Th/U	
	U ppm ^a	Th ppm ^a	²⁰⁷ Pb/ ²³⁵ U	% error	²⁰⁶ Pb/ ²³⁸ U	% error	6/38–7/35	²⁰⁷ Pb/ ²⁰⁶ Pb	% error	38/6–7/6	Age (Ma)	error	Age (Ma)	error	Age (Ma)							error
Hunt (continued)																						
050511-3F-3	281.400	181.500	3.1720	0.0390	0.2532	0.0030	0.9666	0.0910	0.0003	-0.0019	1445.8	38.6	1455	15	1449.4	9.5	1.01	1446	39	1.546		
050511-3F-10	366.500	280.900	3.1710	0.0420	0.2542	0.0032	0.9701	0.0911	0.0003	-0.0766	1448.7	38.5	1462	16	1451	10	1.01	1449	38	1.303		
050511-3F-6	29.820	34.700	3.2150	0.0650	0.2488	0.0044	0.7894	0.0943	0.0011	0.0923	1514.1	43.7	1432	23	1458	16	0.95	1514	44	0.863		
Holbrook																						
103009-1G-11	128.000	148.500	0.2557	0.0063	0.0352	0.0005	0.5932	0.0524	0.0010	-0.0991	304.6	62.4	223	2.8	231.5	5	0.96	223	3	0.860	229 ± 2 Ma	0.91
103009-1G-1	108.900	82.600	0.2545	0.0060	0.0355	0.0005	0.5784	0.0518	0.0010	-0.0384	276.6	63.7	224.6	3	230.5	5	0.97	225	3	1.309		
103009-1G-29	117.600	127.100	0.2530	0.0070	0.0358	0.0005	0.5679	0.0514	0.0012	-0.0886	258.8	70.6	226.5	2.9	228.6	5.7	0.99	227	3	0.926		
103009-1G-27	128.100	191.100	0.2574	0.0052	0.0359	0.0005	0.4540	0.0520	0.0009	0.0984	283.2	61.7	227.3	2.8	232.9	4.3	0.98	227	3	0.673		
103009-1G-6	184.900	346.200	0.2575	0.0050	0.0360	0.0005	0.5923	0.0516	0.0009	0.1123	265.5	59.5	227.8	2.9	232.5	4.1	0.98	228	3	0.535		
103009-1G-17	213.000	374.000	0.2530	0.0049	0.0360	0.0005	0.6098	0.0512	0.0008	0.0624	250.3	57.6	227.9	2.8	229.3	4	0.99	228	3	0.564		
103009-1G-35	148.900	195.900	0.2557	0.0047	0.0361	0.0005	0.5474	0.0512	0.0008	0.1276	251.6	57.0	228.4	2.8	231	3.8	0.99	228	3	0.756		
103009-1G-10	134.600	121.300	0.2775	0.0061	0.0361	0.0005	0.4647	0.0559	0.0010	0.1972	448.4	59.6	228.9	3.1	248.4	4.8	0.92	229	3	1.104		
103009-1G-16	299.700	236.500	0.2548	0.0048	0.0362	0.0005	0.7794	0.0509	0.0006	-0.1548	235.4	53.6	229.1	2.9	230.3	3.9	0.99	229	3	1.271		
103009-1G-28	354.000	429.000	0.2541	0.0052	0.0362	0.0005	0.8456	0.0508	0.0006	-0.1920	230.9	52.7	229.1	3.2	229.7	4.2	1.00	229	3	0.817		
103009-1G-31	131.700	115.700	0.2598	0.0052	0.0362	0.0004	0.3984	0.0517	0.0010	0.1979	270.4	62.6	229.1	2.5	234.3	4.2	0.98	229	3	1.139		
103009-1G-2	401.600	453.900	0.2560	0.0044	0.0362	0.0004	0.7396	0.0516	0.0006	-0.0407	268.2	52.6	229.2	2.7	231.3	3.5	0.99	229	3	0.887		
103009-1G-14	135.700	95.000	0.2720	0.0066	0.0362	0.0005	0.6041	0.0549	0.0010	0.0242	408.2	60.5	229.2	3.2	244	5.3	0.94	229	3	1.431		
103009-1G-21	107.700	252.800	0.2609	0.0062	0.0362	0.0005	0.5913	0.0527	0.0009	-0.1131	313.7	60.4	229.2	2.9	235.1	5	0.97	229	3	0.425		
103009-1G-33	209.500	371.400	0.2535	0.0040	0.0362	0.0004	0.5993	0.0511	0.0007	0.1452	245.8	55.3	229.2	2.7	229.3	3.2	1.00	229	3	0.565		
103009-1G-26	806.500	972.800	0.2561	0.0039	0.0362	0.0005	0.8725	0.0513	0.0004	-0.0808	254.3	49.7	229.3	3.1	231.4	3.2	0.99	229	3	0.827		
103009-1G-9	158.100	221.900	0.2565	0.0057	0.0363	0.0005	0.6238	0.0508	0.0008	0.0007	230.4	59.7	229.5	2.8	232.2	4.6	0.99	230	3	0.708		
103009-1G-19	238.800	234.100	0.2707	0.0048	0.0363	0.0004	0.7145	0.0540	0.0007	-0.1108	371.5	53.2	230	2.3	243.1	3.8	0.95	230	2	1.013		
103009-1G-36	718.200	896.000	0.2597	0.0041	0.0363	0.0005	0.8316	0.0515	0.0004	0.0863	262.4	49.6	230	2.9	234.3	3.3	0.98	230	3	0.799		
103009-1G-4	98.800	60.600	0.2601	0.0059	0.0364	0.0005	0.5390	0.0520	0.0010	-0.0627	285.4	63.1	230.2	2.9	234.5	4.7	0.98	230	3	1.604		
103009-1G-8	198.200	203.600	0.2583	0.0043	0.0365	0.0005	0.5964	0.0516	0.0007	0.1774	265.9	56.5	231.4	2.9	233.2	3.5	0.99	231	3	0.972		
103009-1G-32	545.400	598.000	0.2585	0.0033	0.0367	0.0005	0.8272	0.0507	0.0004	0.1655	228.6	50.2	232.8	3	233.4	2.7	1.00	233	3	0.903		
103009-1G-18	510.500	315.700	0.2711	0.0041	0.0382	0.0005	0.8545	0.0514	0.0005	0.1403	257.0	50.2	241.4	3.4	243.4	3.3	0.99	241	3	1.619		
103009-1G-34	407.000	282.000	0.2755	0.0039	0.0386	0.0005	0.8223	0.0513	0.0005	0.1340	256.1	50.4	244.3	3.3	247	3.1	0.99	244	3	1.438		
103009-1G-7	423.900	323.300	0.2818	0.0046	0.0394	0.0005	0.7960	0.0518	0.0005	0.1213	277.9	51.2	248.8	3.3	251.9	3.7	0.99	249	3	1.312		
103009-1G-37	273.500	128.000	0.3028	0.0050	0.0423	0.0006	0.7281	0.0518	0.0006	0.1591	276.1	51.9	267	3.5	268.4	3.9	0.99	267	4	2.120		
103009-1G-20	391.700	38.200	0.3258	0.0045	0.0448	0.0006	0.8128	0.0526	0.0004	0.1848	313.3	49.3	282.5	3.8	286.2	3.5	0.99	283	4	10.470		
103009-1G-3	410.800	262.600	0.5998	0.0090	0.0770	0.0010	0.8924	0.0567	0.0004	0.0365	481.4	46.4	477.8	6.3	477.4	5.6	1.00	478	6	1.564		
103009-1G-15	603.000	180.500	1.0130	0.0180	0.1048	0.0018	0.9697	0.0699	0.0003	-0.0958	924.5	42.0	643	10	710.6	9.4	0.90	643	10	3.313		
103009-1G-30	371.300	566.000	3.1290	0.0470	0.2469	0.0037	0.9745	0.0916	0.0003	-0.0602	1458.7	38.6	1422	19	1440	11	0.97	1459	39	0.650		
103009-1G-23	248.900	131.500	4.0240	0.0570	0.2881	0.0039	0.9658	0.1011	0.0004	-0.1333	1643.5	37.7	1631	20	1639	11	0.99	1643	38	1.903		
103009-1G-12	442.600	383.700	4.1230	0.0530	0.2913	0.0037	0.9857	0.1027	0.0002	-0.0909	1672.6	37.2	1648	18	1658	11	0.99	1673	37	1.149		
103009-1G-5	558.300	252.700	0.3478	0.0060	0.0406	0.0005	0.7000	0.0624	0.0008	0.0698	687.8	49.8	256.3	3.2	303.3	4.5	0.37	discordant	50	2.210		
103009-1G-13	114.400	173.200	0.3720	0.0310	0.0390	0.0006	0.7514	0.0695	0.0052	-0.6242	913.6	159.4	246.6	4	316	22	0.27	discordant	159	0.669		
103009-1G-22	547.500	173.200	2.5660	0.0640	0.1888	0.0045	0.9927	0.0986	0.0004	-0.4222	1597.4	37.9	1114	24	1290	19	0.70	discordant	38	3.210		
103009-1G-24	45.500	72.600	0.3100	0.0110	0.0376	0.0005	0.4625	0.0605	0.0017	-0.0394	621.5	74.4	238.1	3.1	274.5	8.5	0.38	discordant	74	0.624		



(continued)

TABLE 2A. LA-ICPMS U-Pb ZIRCON DATA FOR SHINARUMP CONGLOMERATE CLASTS (continued)

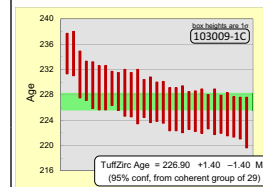
Sample location and number	Measured isotopic ratios		Isotopic ages ^b						Concordance Filter	Best age (Ma)	error	Th/U	Clast age	Average clast Th/U								
	U ppm ^a	Th ppm ^a	²⁰⁷ Pb/ ²³⁵ U	% error	²⁰⁶ Pb/ ²³⁸ U	% error	Error Correlation 6/38–7/35	²⁰⁷ Pb/ ²⁰⁶ Pb							% error	Error Correlation 38/6–7/6	Age (Ma)	error	Age (Ma)	error	Age (Ma)	error
Holbrook (continued)																						
052111-1A-16	131.700	136.500	0.2494	0.0062	0.0358	0.0005	0.6385	0.0501	0.0010	-0.0378	199.6	65.6	226.7	3.1	225.8	5.1	1.00	227	3	1.043	230 ± 2 Ma	1.05
052111-1A-6	161.800	237.100	0.2519	0.0052	0.0358	0.0005	0.5211	0.0503	0.0009	0.1612	208.9	60.7	226.8	3.1	228.5	4.1	0.99	227	3	1.485		
052111-1A-29	89.200	73.900	0.2598	0.0072	0.0358	0.0004	0.4423	0.0519	0.0012	0.0315	281.0	70.0	226.9	2.7	234.1	5.8	0.97	227	3	0.845		
052111-1A-19	182.400	178.000	0.2572	0.0049	0.0359	0.0005	0.6779	0.0517	0.0008	0.1066	273.1	56.6	227	3.3	232.3	4	0.98	227	3	0.995		
052111-1A-1	128.000	97.600	0.2590	0.0056	0.0360	0.0005	0.6470	0.0525	0.0009	0.0142	305.5	59.2	227.8	3.3	233.6	4.5	0.98	228	3	0.767		
052111-1A-2	165.000	194.700	0.2553	0.0050	0.0360	0.0006	0.6794	0.0510	0.0008	0.1258	239.9	58.1	227.9	3.7	230.7	4	0.99	228	4	1.186		
052111-1A-18	290.000	277.200	0.2576	0.0049	0.0360	0.0005	0.7778	0.0515	0.0006	-0.0918	262.8	53.4	228.2	3.1	233	4	0.98	228	3	0.962		
052111-1A-22	133.000	177.300	0.2549	0.0058	0.0361	0.0004	0.6187	0.0509	0.0009	-0.1580	237.7	61.9	228.3	2.7	230.3	4.7	0.99	228	3	1.312		
052111-1A-5	103.500	67.050	0.2621	0.0057	0.0360	0.0005	0.4441	0.0530	0.0011	0.2159	328.8	65.4	228.4	3.1	236.7	4.5	0.96	228	3	0.654		
052111-1A-28	204.100	170.100	0.2542	0.0044	0.0361	0.0004	0.6459	0.0511	0.0006	0.0672	245.8	54.1	228.7	2.7	230.7	3.5	0.99	229	3	0.846		
052111-1A-24	220.600	267.700	0.2539	0.0044	0.0362	0.0004	0.6937	0.0508	0.0007	-0.0163	229.9	55.3	229.1	2.6	229.6	3.6	1.00	229	3	1.243		
052111-1A-7	107.000	148.400	0.2577	0.0061	0.0362	0.0005	0.4317	0.0524	0.0011	0.1252	302.9	66.1	229.3	3	233.2	5	0.98	229	3	1.403		
052111-1A-10	148.800	234.500	0.2549	0.0055	0.0363	0.0005	0.5788	0.0509	0.0009	0.0479	234.5	62.2	229.7	3	230.9	4.5	0.99	230	3	1.575		
052111-1A-20	247.500	169.400	0.2583	0.0050	0.0363	0.0005	0.6165	0.0510	0.0007	0.1689	240.4	56.7	229.8	3.3	233.1	4	0.99	230	3	0.696		
052111-1A-13	186.100	165.200	0.2593	0.0054	0.0363	0.0004	0.7202	0.0517	0.0008	-0.2163	269.9	57.7	230.1	2.7	233.9	4.3	0.98	230	3	0.901		
052111-1A-25	125.000	93.600	0.2551	0.0053	0.0364	0.0005	0.5834	0.0510	0.0009	0.0571	242.2	62.4	230.1	3.3	230.5	4.3	1.00	230	3	0.760		
052111-1A-26	81.230	96.900	0.2529	0.0070	0.0364	0.0005	0.2255	0.0501	0.0014	0.2564	199.6	79.8	230.3	3	228.6	5.7	1.01	230	3	1.215		
052111-1A-12	202.900	201.000	0.2563	0.0053	0.0364	0.0005	0.7451	0.0510	0.0007	-0.1526	242.2	55.1	230.4	2.8	231.5	4.3	1.00	230	3	0.986		
052111-1A-11	187.200	141.500	0.2560	0.0043	0.0365	0.0005	0.5862	0.0507	0.0008	0.0651	227.2	58.9	231	2.9	231.8	3.6	1.00	231	3	0.767		
052111-1A-27	99.900	139.000	0.2531	0.0082	0.0365	0.0006	0.6498	0.0504	0.0012	0.0041	213.5	72.0	231.1	3.7	229.5	6.5	1.01	231	4	1.374		
052111-1A-4	140.000	185.100	0.2568	0.0054	0.0366	0.0005	0.6821	0.0512	0.0008	-0.0805	247.6	58.7	231.6	3.1	232.4	4.5	1.00	232	3	1.335		
052111-1A-3	151.200	171.700	0.2589	0.0059	0.0366	0.0005	0.6645	0.0518	0.0009	-0.1007	276.1	61.3	231.7	3.2	234.1	4.6	0.99	232	3	1.143		
052111-1A-14	131.100	101.600	0.2577	0.0056	0.0366	0.0005	0.5584	0.0516	0.0009	0.0748	266.4	61.5	231.7	3.1	232.6	4.5	1.00	232	3	0.785		
052111-1A-9	146.100	199.300	0.2585	0.0054	0.0368	0.0006	0.5797	0.0509	0.0009	0.1574	234.9	62.8	232.9	3.5	233.3	4.4	1.00	233	4	1.378		
052111-1A-15	192.000	199.900	0.2599	0.0052	0.0368	0.0005	0.5608	0.0517	0.0009	0.0721	273.1	61.0	232.9	2.9	234.4	4.2	0.99	233	3	1.063		
052111-1A-17	559.000	292.000	0.2686	0.0046	0.0370	0.0005	0.8569	0.0523	0.0005	-0.0845	296.4	49.9	234	3.2	241.4	3.6	0.97	234	3	0.530		
052111-1A-21	293.500	170.300	0.2398	0.0037	0.0340	0.0004	0.6573	0.0509	0.0006	0.1250	234.5	54.3	215.7	2.6	218.5	3	0.99	216	3	0.590		
052111-1A-23	421.900	673.300	3.2340	0.0410	0.2557	0.0032	0.9735	0.0914	0.0003	-0.1055	1454.3	38.5	1467	16	1464.4	9.8	1.01	1454	38	1.620		
052111-1A-8	387.000	294.600	3.2280	0.0440	0.2561	0.0035	0.9788	0.0918	0.0002	0.1600	1463.3	38.3	1470	18	1465	11	1.00	1463	38	0.778		
052111-1A-30	332.600	161.700	3.8670	0.0430	0.2787	0.0030	0.9732	0.1004	0.0003	0.1280	1631.3	37.6	1584	15	1606.1	8.9	0.97	1631	38	0.495		
232 ± 2 Ma																						
052111-1C-9	97.200	182.000	0.2549	0.0074	0.0359	0.0006	0.6836	0.0517	0.0010	-0.1041	272.2	63.8	227.2	3.8	230.1	5.9	0.99	227	4	1.867	232 ± 2 Ma	1.46
052111-1C-20	209.000	231.000	0.2533	0.0053	0.0361	0.0006	0.7652	0.0516	0.0007	0.0439	269.1	55.7	228.4	3.9	229	4.3	1.00	228	4	1.148		
052111-1C-8	158.400	400.000	0.2710	0.0063	0.0363	0.0005	0.6464	0.0537	0.0009	-0.0039	359.3	58.9	229.7	3.4	243.2	5.1	0.94	230	3	2.506		
052111-1C-4	128.600	263.200	0.2609	0.0063	0.0363	0.0005	0.5381	0.0524	0.0011	0.0791	302.9	66.1	229.8	3.3	235.1	5	0.98	230	3	2.077		
052111-1C-1	364.900	463.300	0.2587	0.0043	0.0364	0.0005	0.8023	0.0512	0.0006	-0.0564	247.6	52.5	230.6	3.2	233.5	3.5	0.99	231	3	1.256		
052111-1C-10	110.400	212.800	0.2639	0.0060	0.0364	0.0005	0.6307	0.0527	0.0009	0.0480	315.9	60.7	230.7	3.2	238.1	4.7	0.97	231	3	1.938		
052111-1C-11	132.100	163.100	0.2619	0.0059	0.0365	0.0005	0.6425	0.0517	0.0009	-0.0359	271.7	61.1	230.9	3.3	236.5	4.9	0.98	231	3	1.241		
052111-1C-2	224.700	348.500	0.2568	0.0046	0.0365	0.0004	0.6859	0.0509	0.0007	-0.0428	236.8	55.5	231.3	2.5	231.9	3.7	1.00	231	3	1.561		
052111-1C-22	61.900	100.000	0.2615	0.0093	0.0366	0.0006	0.3731	0.0520	0.0016	0.0357	285.4	83.9	231.5	3.9	236.3	7.6	0.98	232	4	1.567		
052111-1C-15	70.100	58.600	0.2668	0.0084	0.0365	0.0007	0.4857	0.0532	0.0015	0.0972	337.3	78.3	231.7	4	239.6	6.7	0.97	232	4	0.843		
052111-1C-17	337.000	396.000	0.2542	0.0045	0.0366	0.0005	0.7822	0.0499	0.0006	0.0590	192.2	53.1	231.8	3.3	230.3	3.5	1.01	232	3	1.170		
052111-1C-24	191.800	349.000	0.2602	0.0053	0.0367	0.0006	0.7155	0.0512	0.0007	0.0808	250.3	56.3	232.4	3.7	234.6	4.3	0.99	232	4	1.792		
052111-1C-21	340.900	253.200	0.2553	0.0048	0.0368	0.0005	0.7880	0.0504	0.0005	0.0128	212.6	52.4	232.6	3.3	230.7	3.9	1.01	233	3	0.745		



(continued)

TABLE 2A. LA-ICPMS U-Pb ZIRCON DATA FOR SHINARUMP CONGLOMERATE CLASTS (continued)

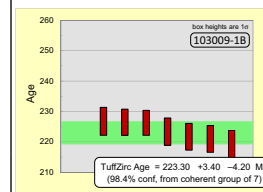
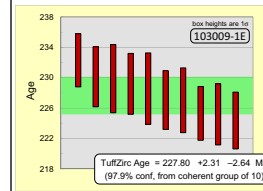
Sample location and number	U ppm ^a		Th ppm ^a		Measured isotopic ratios						Isotopic ages ^b						Concordance Filter	Best age (Ma)	error	Th/U	Clast age	Average clast Th/U
	U ppm ^a	Th ppm ^a	²⁰⁷ Pb/ ²³⁵ U	% error	²⁰⁶ Pb/ ²³⁸ U	% error	6/38–7/35	²⁰⁷ Pb/ ²⁰⁶ Pb	% error	38/6–7/6	Age (Ma)	error	Age (Ma)	error	Age (Ma)	error						
Holbrook (continued)																						
052111-1C-16	429.900	304.000	0.2552	0.0044	0.0368	0.0005	0.8891	0.0506	0.0004	-0.0328	223.1	50.3	232.8	3.4	231.6	3.5	1.01	233	3	0.693	227 ± 2 Ma	0.87
052111-1C-12	820.000	1160.000	0.2916	0.0059	0.0370	0.0006	0.6642	0.0567	0.0010	0.0405	481.1	57.9	234	3.8	259.6	4.6	0.90	234	4	1.433		
052111-1C-18	309.700	348.600	0.2532	0.0046	0.0369	0.0006	0.7999	0.0505	0.0006	0.1317	216.7	53.9	234.1	3.8	229	3.8	1.02	234	4	1.131		
052111-1C-23	97.900	204.500	0.2572	0.0067	0.0371	0.0006	0.6425	0.0506	0.0011	-0.0755	222.6	68.3	234.7	3.6	233.5	5.2	1.01	235	4	2.106		
052111-1C-19	101.500	162.200	0.2598	0.0074	0.0371	0.0007	0.6232	0.0508	0.0012	0.0611	231.8	71.5	234.8	4.3	234.2	6	1.00	235	4	1.609		
052111-1C-13	567.900	625.300	0.2638	0.0045	0.0373	0.0006	0.9175	0.0518	0.0005	0.0838	274.8	50.0	235.7	3.9	237.6	3.6	0.99	236	4	1.106		
052111-1C-5	88.300	160.800	0.2702	0.0070	0.0378	0.0006	0.4768	0.0520	0.0012	0.1034	285.4	69.8	239.3	3.4	243.2	5.5	0.98	239	3	1.792		
052111-1C-3	240.000	294.000	0.2325	0.0047	0.0308	0.0004	0.7809	0.0547	0.0007	-0.0909	398.8	54.1	195.4	2.8	212.1	3.8	0.92	195	3	1.244		
052111-1C-14	513.000	219.300	3.1500	0.0470	0.2515	0.0037	0.9848	0.0911	0.0002	0.1665	1448.9	38.4	1446	19	1448	12	1.00	1449	38	0.427		
052111-1C-6	24.300	78.100	0.4640	0.0250	0.0404	0.0011	0.6461	0.0828	0.0038	-0.1428	1264.5	97.8	255.1	6.5	384	17	0.20	discordant	98	3.218		
052111-1C-7	129.400	191.600	0.4460	0.0240	0.0363	0.0010	-0.5405	0.0911	0.0073	0.7873	1448.7	157.2	229.9	6.5	371	16	0.16	discordant	157	1.567		
103009-1C-24	132.900	175.600	0.2436	0.0065	0.0353	0.0006	0.7388	0.0501	0.0009	-0.0179	198.2	62.8	223.6	4	221.7	5.4	1.01	224	4	1.316		
103009-1C-12	265.400	224.000	0.2457	0.0053	0.0354	0.0005	0.6916	0.0506	0.0008	-0.0071	223.6	59.8	224.3	3.3	222.9	4.3	1.01	224	3	0.847		
103009-1C-11	197.500	123.600	0.2491	0.0050	0.0355	0.0005	0.6835	0.0511	0.0008	-0.0323	243.1	58.3	224.5	3.2	225.7	4	0.99	225	3	0.628		
103009-1C-4	143.500	104.400	0.2501	0.0053	0.0355	0.0005	0.6673	0.0502	0.0008	-0.1207	202.0	60.0	224.9	3	226.5	4.3	0.99	225	3	0.723		
103009-1C-23	320.700	276.500	0.2470	0.0046	0.0355	0.0005	0.7657	0.0504	0.0006	0.0278	214.4	53.4	224.9	3.4	224	3.8	1.00	225	3	0.860		
103009-1C-1	299.500	287.800	0.2489	0.0041	0.0356	0.0004	0.7190	0.0507	0.0005	-0.0085	227.7	52.4	225.3	2.7	226	3.3	1.00	225	3	0.969		
103009-1C-10	119.700	71.600	0.2467	0.0059	0.0356	0.0006	0.7350	0.0503	0.0008	-0.1291	207.0	59.6	225.3	3.6	223.6	4.8	1.01	225	4	0.597		
103009-1C-13	120.400	148.900	0.2509	0.0063	0.0356	0.0005	0.5746	0.0508	0.0010	0.0533	233.1	63.2	225.4	3.2	227	5.1	0.99	225	3	1.247		
103009-1C-29	249.900	226.500	0.2532	0.0051	0.0356	0.0006	0.7199	0.0513	0.0008	0.1121	254.8	57.5	225.4	3.5	229	4.1	0.98	225	4	0.914		
103009-1C-8	207.000	179.600	0.2424	0.0045	0.0356	0.0005	0.6249	0.0499	0.0007	0.1246	188.0	56.9	225.5	3	220.3	3.7	1.02	226	3	0.867		
103009-1C-2	147.600	127.700	0.2523	0.0057	0.0356	0.0005	0.7014	0.0514	0.0008	0.0560	257.9	58.0	225.7	3.4	229.3	4.6	0.98	226	3	0.868		
103009-1C-14	198.800	103.000	0.2490	0.0046	0.0356	0.0006	0.7397	0.0511	0.0006	0.0392	246.7	54.1	225.7	3.4	226	3.7	1.00	226	3	0.518		
103009-1C-21	83.900	62.500	0.2593	0.0060	0.0356	0.0006	0.5209	0.0526	0.0011	0.1879	311.6	65.9	225.7	3.7	233.9	4.9	0.96	226	4	0.747		
103009-1C-9	131.700	86.800	0.2523	0.0056	0.0358	0.0005	0.5541	0.0514	0.0009	0.1350	257.5	62.0	226.8	3.3	228.8	4.4	0.99	227	3	0.654		
103009-1C-22	175.200	111.900	0.2539	0.0043	0.0358	0.0005	0.5534	0.0510	0.0008	0.2207	240.4	58.3	226.9	3.1	229.6	3.5	0.99	227	3	0.637		
103009-1C-15	192.500	209.800	0.2474	0.0053	0.0359	0.0006	0.7954	0.0500	0.0007	-0.0680	196.4	56.2	227.2	3.6	224.2	4.3	1.01	227	4	1.087		
103009-1C-18	73.800	42.260	0.2535	0.0063	0.0359	0.0005	0.5358	0.0524	0.0012	0.0696	302.9	69.3	227.4	3	229.2	5.1	0.99	227	3	0.568		
103009-1C-7	247.000	298.000	0.2487	0.0051	0.0360	0.0007	0.8532	0.0500	0.0006	0.0099	196.9	54.4	227.7	4.3	225.4	4.1	1.01	228	4	1.148		
103009-1C-17	170.000	100.500	0.2571	0.0046	0.0360	0.0006	0.6636	0.0514	0.0008	0.0598	260.1	57.4	228	3.5	232.2	3.7	0.98	228	4	0.592		
103009-1C-27	202.900	155.400	0.2489	0.0047	0.0361	0.0006	0.7780	0.0504	0.0006	0.1657	211.2	53.5	228.3	3.7	225.6	3.8	1.01	228	4	0.773		
103009-1C-20	130.800	81.200	0.2543	0.0058	0.0361	0.0005	0.5953	0.0510	0.0010	-0.0063	239.0	63.0	228.5	3	229.8	4.7	0.99	229	3	0.625		
103009-1C-5	224.000	209.000	0.2524	0.0046	0.0362	0.0004	0.6343	0.0510	0.0008	0.0256	242.2	57.2	229	2.7	228.4	3.7	1.00	229	3	0.914		
103009-1C-25	209.300	215.700	0.2572	0.0050	0.0362	0.0006	0.7252	0.0516	0.0006	0.1960	265.5	54.0	229.1	3.5	233.5	4	0.98	229	4	1.019		
103009-1C-26	236.400	191.500	0.2574	0.0055	0.0362	0.0006	0.8024	0.0513	0.0006	-0.1793	252.1	53.8	229.1	3.5	232.3	4.4	0.99	229	4	0.803		
103009-1C-28	194.200	300.500	0.2591	0.0063	0.0362	0.0006	0.6444	0.0513	0.0008	0.0413	253.0	58.9	229.5	3.7	233.6	5	0.98	230	4	1.552		
103009-1C-19	193.000	163.400	0.2624	0.0052	0.0364	0.0005	0.7186	0.0524	0.0007	0.0168	304.6	54.8	230.2	3.1	236.4	4.2	0.97	230	3	0.855		
103009-1C-6	122.500	79.600	0.2495	0.0057	0.0365	0.0006	0.6084	0.0500	0.0009	0.0831	194.1	63.5	231.2	3.7	226.6	4.8	1.02	231	4	0.651		
103009-1C-3	113.900	104.500	0.2554	0.0064	0.0370	0.0005	0.6357	0.0508	0.0009	-0.1110	230.4	62.9	234.5	3.2	231.3	5.3	1.01	235	3	0.923		
103009-1C-16	167.600	213.700	0.2576	0.0047	0.0371	0.0006	0.6692	0.0507	0.0007	0.1941	224.9	57.3	234.5	3.5	232.6	3.8	1.01	235	4	1.277		



(continued)

TABLE 2A. LA-ICPMS U-Pb ZIRCON DATA FOR SHINARUMP CONGLOMERATE CLASTS (continued)

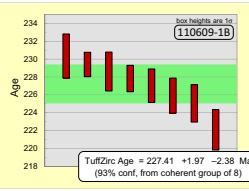
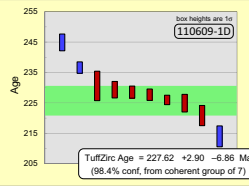
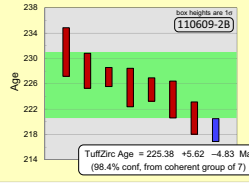
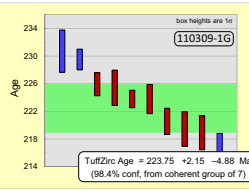
Sample location and number	U ppm ^a		Th ppm ^a		Measured isotopic ratios						Isotopic ages ^b						Concordance Filter	Best age (Ma)	error	Th/U	Clast age	Average clast Th/U
	U ppm ^a	Th ppm ^a	²⁰⁷ Pb/ ²³⁵ U	% error	²⁰⁶ Pb/ ²³⁸ U	% error	Error Correlation 6/38-7/35	Error Correlation 207Pb/ ²⁰⁶ Pb	% error	Age (Ma)	Age (Ma)	Age (Ma)	error	error	error	error						
Holbrook (continued)																						
103009-1E-6	297.544	305.981	0.2495	0.0050	0.0354	0.0006	0.7661	0.0508	0.0006	0.1868	229.9	54.5	224.3	3.7	226.9	3.9	0.99	224	4	1.047	228 ± 3 Ma	1.17
103009-1E-3	530.275	534.091	0.2505	0.0054	0.0355	0.0006	0.8866	0.0511	0.0005	-0.0624	246.7	51.3	225.2	4.0	227.2	4.3	0.99	225	4	1.045		
103009-1E-2	245.908	295.778	0.2498	0.0044	0.0356	0.0006	0.6790	0.0509	0.0007	0.1900	236.6	56.7	225.3	3.5	226.7	3.6	0.99	225	4	1.214		
103009-1E-7	113.919	144.307	0.2566	0.0067	0.0358	0.0007	0.5660	0.0521	0.0010	0.1360	288.9	64.8	227.0	4.3	231.5	5.5	0.98	227	4	1.279		
103009-1E-4	203.789	174.075	0.2496	0.0058	0.0359	0.0006	0.7636	0.0512	0.0008	0.0275	248.2	58.2	227.0	3.9	226.5	4.7	1.00	227	4	0.864		
103009-1E-8	245.217	408.749	0.2538	0.0060	0.0361	0.0008	0.7789	0.0514	0.0008	0.0705	256.6	58.0	228.5	4.7	229.9	4.8	0.99	229	5	1.688		
103009-1E-9	148.669	250.448	0.2543	0.0068	0.0362	0.0006	0.6556	0.0509	0.0011	0.0066	236.8	66.6	229.2	4.0	230.2	5.6	1.00	229	4	1.697		
103009-1E-1	175.304	139.289	0.2484	0.0075	0.0363	0.0007	0.7754	0.0500	0.0009	-0.0895	196.2	63.1	229.9	4.5	225.4	6.1	1.02	230	4	0.803		
103009-1E-11	537.462	543.710	0.2542	0.0053	0.0363	0.0006	0.9105	0.0512	0.0006	0.0993	251.9	52.2	230.1	4.0	229.7	4.3	1.00	230	4	1.016		
103009-1E-5	173.596	175.267	0.2680	0.0054	0.0367	0.0006	0.5713	0.0528	0.0008	0.1117	319.4	57.4	232.3	3.5	240.8	4.3	0.96	232	4	1.029		
103009-1E-10	196.093	88.338	3.1149	0.0659	0.2498	0.0050	0.9736	0.0904	0.0004	-0.0610	1433.6	39.2	1438.7	25.5	1432.9	16.1	1.00	1434	39	0.454		
103009-1K-7	459.000	650.000	0.2527	0.0055	0.0357	0.0008	0.9246	0.0511	0.0005	-0.0085	243.1	50.4	225.8	4.7	228.5	4.5	0.99	226	5	1.431	Median age 228 Ma	1.24
103009-1K-4	308.500	414.000	0.2513	0.0053	0.0358	0.0006	0.8523	0.0505	0.0006	-0.0993	219.4	54.1	226.9	3.6	227.5	4.3	1.00	227	4	1.330		
103009-1K-2	439.600	761.400	0.2566	0.0052	0.0360	0.0007	0.8623	0.0513	0.0005	0.0921	253.0	51.8	228.2	4.2	232.2	4.3	0.98	228	4	1.719		
103009-1K-6	547.300	505.000	0.2525	0.0052	0.0360	0.0007	0.9007	0.0506	0.0004	0.0129	224.5	49.9	228.4	4	229.4	4.2	1.00	228	4	0.925		
103009-1K-1	589.800	483.700	0.2593	0.0052	0.0365	0.0007	0.9061	0.0514	0.0005	0.0497	257.9	50.5	231.2	4.1	234.4	4.2	0.99	231	4	0.806		
103009-1K-5	94.400	70.100	3.0620	0.0580	0.2432	0.0044	0.9472	0.0908	0.0006	-0.0922	1442.8	40.1	1402	23	1421	14	0.97	1443	40	0.741		
103009-1K-3	67.130	67.400	11.1700	0.2400	0.4673	0.0096	0.9731	0.1721	0.0008	-0.1143	2577.8	34.3	2469	42	2538	20	0.96	2578	34	0.991		
103009-1H-4	518.000	525.000	0.2566	0.0046	0.0354	0.0006	0.8400	0.0518	0.0005	-0.0540	277.5	51.2	224.2	3.6	231.8	3.7	0.97	224	4	1.035	Median age 227 Ma	1.60
103009-1H-1	57.590	72.400	0.2571	0.0087	0.0358	0.0008	0.5666	0.0520	0.0014	0.1418	285.4	76.7	226.8	5	231.9	7	0.98	227	5	1.256		
103009-1H-3	125.400	300.000	0.2610	0.0056	0.0359	0.0006	0.4854	0.0528	0.0010	0.2682	318.5	61.2	227	3.8	235.2	4.5	0.97	227	4	2.391		
103009-1H-2	270.600	462.200	0.2589	0.0051	0.0361	0.0007	0.8094	0.0516	0.0007	0.0637	269.1	54.2	228.7	4.1	233.6	4.1	0.98	229	4	1.735		
103009-1B-6	403.000	405.000	0.2468	0.0063	0.0346	0.0007	0.8987	0.0519	0.0006	-0.1432	279.7	52.4	219.1	4.6	224.3	5.1	0.98	219	5	1.021	223 ± 4 Ma	1.37
103009-1B-1	213.800	276.700	0.2540	0.0065	0.0349	0.0007	0.7969	0.0527	0.0008	0.0955	315.0	55.8	220.9	4.4	229.5	5.3	0.96	221	4	1.314		
103009-1B-5	156.800	256.700	0.2535	0.0068	0.0350	0.0007	0.7641	0.0525	0.0009	-0.0054	308.5	60.3	221.6	4.4	229.1	5.5	0.97	222	4	1.648		
103009-1B-4	487.000	1310.000	0.2492	0.0054	0.0353	0.0007	0.9038	0.0514	0.0005	0.0403	256.6	51.3	223.3	4.5	225.7	4.4	0.99	223	5	2.732		
103009-1B-11	191.600	189.400	0.2496	0.0054	0.0357	0.0007	0.7281	0.0512	0.0008	0.1981	249.8	57.1	226.2	4.1	226.1	4.3	1.00	226	4	0.985		
103009-1B-10	654.000	580.000	0.2489	0.0053	0.0358	0.0007	0.9089	0.0504	0.0005	0.1040	214.9	50.7	226.4	4.3	225.5	4.3	1.00	226	4	0.886		
103009-1B-8	363.700	350.300	0.2514	0.0065	0.0358	0.0007	0.8805	0.0511	0.0005	-0.1599	244.0	51.9	226.7	4.6	227.4	5.2	1.00	227	5	0.976		
103009-1B-2	219.400	81.300	3.4820	0.0690	0.2655	0.0056	0.9773	0.0947	0.0004	0.1065	1521.9	38.6	1523	28	1520	16	1.00	1522	39	0.376		
103009-1B-9	553.000	311.000	4.1450	0.0920	0.2716	0.0057	0.9926	0.1107	0.0003	-0.4764	1811.3	36.7	1547	29	1660	18	0.85	1811	37	0.567		
103009-1B-7	375.500	218.300	5.0500	0.1100	0.3200	0.0068	0.9904	0.1143	0.0003	0.1561	1868.6	36.5	1792	34	1824	18	0.96	1869	36	0.585		
103009-1B-3	280.000	206.400	2.7700	0.0730	0.1957	0.0046	0.9844	0.1031	0.0005	-0.2512	1680.8	38.1	1154	24	1360	19	0.69	discordant	38	0.722		



^aConcentration data are normalized to the primary reference material (91500) and are accurate to ~ 10%.
^bConcentration data are normalized to the primary reference material (91500) and are accurate to ~ 10%.
^c²⁰⁷Pb/²³⁵U calculated assuming a natural ²³⁵U/²³⁸U ratio of 137.88.
^dDiscordancy is measured by ²⁰⁶Pb/²³⁸U / ²⁰⁷Pb/²³⁵U for grains > 1000 Ma and ²⁰⁶Pb/²³⁸U / ²⁰⁷Pb/²⁰⁶Pb for grains < 1000 Ma.
^eAge calculations are based on the decay constants of Jaffey et al. (1971).

TABLE 2B. SHRIMP-RG U-Pb ZIRCON DATA FOR SHINARUMP CONGLOMERATE CLASTS

For the full-sized version of Table 2B, please visit <http://dx.doi.org/10.1130/GES01238.S3> or the full-text article on www.gsapubs.org.

	U ppm Th ppm		Measured isotopic ratios									Isotopic ages (Ma)								Concordance filter [§]	Best age (Ma)	error	Th/U	Clast age	Average clast Th/U		
			²³⁸ U/ ²⁰⁶ Pb			[common Pb corrected]			error correlation			²⁰⁶ Pb*/ ²³⁸ U		²⁰⁷ Pb*/ ²³⁵ U		error	age	error	age								error
			% error	²⁰⁷ Pb/ ²⁰⁶ Pb	% error	²⁰⁷ Pb/ ²³⁵ U	% error	²⁰⁶ Pb/ ²³⁸ U	% error	6/387/35	²⁰⁶ Pb*/ ²³⁸ U	error	age	error	age												
Cameron																											
110609-1B-2	178	202	28.5212	1.01	0.0509	3.16	0.2460	3.3	0.0351	1.01	0.30	235	73	222	2	223	7	1.01	222	2	1.134	227 ± 2 Ma	1.36				
110609-1B-1	211	230	28.1356	0.91	0.0511	3.78	0.2502	3.9	0.0355	0.91	0.23	244	87	225	2	227	9	1.01	225	2	1.087						
110609-1B-7	238	245	28.0159	0.86	0.0514	2.73	0.2395	4.0	0.0356	0.87	0.22	139	91	226	2	218	9	0.97	226	2	1.027						
110609-1B-6	275	402	27.9094	0.82	0.0504	2.55	0.2372	3.7	0.0357	0.83	0.23	107	84	227	2	216	8	0.95	227	2	1.460						
110609-1B-9	456	1100	27.7506	0.64	0.0521	2.01	0.2591	2.1	0.0360	0.64	0.30	292	46	228	1	234	5	1.03	228	1	2.412						
110609-1B-8	201	184	27.6035	0.94	0.0536	2.90	0.2505	5.2	0.0361	0.98	0.19	212	119	229	2	227	12	0.99	229	2	0.918						
110609-1B-5	506	739	27.5749	0.59	0.0517	1.85	0.2583	1.9	0.0363	0.59	0.31	270	42	229	1	233	5	1.02	229	1	1.458						
110609-1B-4	155	212	27.4082	1.05	0.0532	4.07	0.2594	4.7	0.0364	1.06	0.22	271	105	230	2	234	11	1.02	230	2	1.369						
110609-1B-3	168	198	28.3440	1.01	0.0531	3.15	0.2027	11.2	0.0348	1.15	0.10	-212	280	223	2	187	21	0.84	discordant	2							
110609-1D																											
110609-1D-4	77	82	29.5783	1.59	0.0520	5.52	0.2132	10.8	0.0336	1.66	0.15	2	257	214	3	196	21	0.92	214	3	1.062	228 ± 7 Ma	1.46				
110609-1D-9	90	172	28.5663	1.43	0.0544	7.72	0.2466	9.2	0.0349	1.45	0.16	254	209	221	3	224	21	1.01	221	3	1.908						
110609-1D-5	109	184	28.0485	1.28	0.0542	3.91	0.2665	4.1	0.0357	1.28	0.31	380	88	225	3	240	10	1.07	225	3	1.692						
110609-1D-13	388	1219	28.0164	0.68	0.0513	2.16	0.2525	2.3	0.0357	0.68	0.30	255	50	226	2	229	5	1.01	226	2	3.141						
110609-1D-10	265	347	27.7993	0.82	0.0514	2.58	0.2392	5.0	0.0358	0.86	0.17	119	117	228	2	218	11	0.96	228	2	1.306						
110609-1D-7	316	430	27.6679	0.87	0.0522	2.34	0.2558	2.7	0.0361	0.87	0.32	258	59	228	2	231	6	1.01	228	2	1.360						
110609-1D-1	131	227	27.4505	1.17	0.0556	3.54	0.2607	5.0	0.0363	1.19	0.24	291	111	229	3	235	12	1.03	229	3	1.738						
110609-1D-15	54	72	27.4648	2.02	0.0508	10.75	0.2324	13.4	0.0362	2.04	0.15	26	317	231	5	212	28	0.92	231	5	1.341						
110609-1D-11	280	194	26.8247	0.79	0.0488	2.59	0.2431	3.6	0.0372	0.80	0.22	68	83	237	2	221	8	0.93	237	2	0.695						
110609-1D-3	137	45	25.8074	1.12	0.0518	3.48	0.2769	3.7	0.0387	1.12	0.31	278	80	245	3	248	9	1.01	245	3	0.328						
110609-1D-2	204	144	3.9907	0.64	0.0905	0.87	3.1187	1.1	0.2505	0.64	0.59	1432	17	1442	9	1437	16	1.00	1432	17	0.704						
110609-1D-6	51	36	29.2040	1.92	0.0585	5.79	0.1968	19.9	0.0336	2.14	0.11	-195	495	215	4	182	36	0.85	discordant	4							
110609-1D-8	52	90	28.9717	1.76	0.0598	5.20	0.2011	19.2	0.0338	1.99	0.10	-160	474	216	4	186	36	0.86	discordant	4							
110609-1D-12	94	131	28.3059	1.38	0.0509	4.42	0.1699	16.9	0.0347	1.54	0.09	-666	464	222	3	159	27	0.72	discordant	3							
110609-1D-14	168	180	28.5756	1.06	0.0508	3.41	0.2148	7.2	0.0347	1.11	0.15	-63	174	224	2	198	14	0.88	discordant	2							
110609-2B																											
110609-2B-10	243	251	28.9647	0.82	0.0510	2.61	0.2285	3.9	0.0344	0.83	0.21	108	91	219	2	209	8	0.96	219	2	1.033	225 ± 6 Ma	1.64				
110609-2B-5	134	160	28.7658	1.15	0.0496	3.68	0.2377	3.9	0.0348	1.15	0.30	175	86	221	3	216	8	0.98	221	3	1.191						
110609-2B-4	137	239	28.1761	1.29	0.0554	3.76	0.2375	7.5	0.0352	1.34	0.18	144	173	223	3	216	16	0.97	223	3	1.744						
110609-2B-2	257	898	28.1293	0.81	0.0511	2.58	0.2426	3.2	0.0355	0.82	0.26	176	72	225	2	221	7	0.98	225	2	3.490						
110609-2B-3	93	100	28.0279	1.34	0.0529	4.17	0.2470	5.6	0.0356	1.35	0.24	212	126	225	3	224	13	0.99	225	3	1.072						
110609-2B-9	429	695	27.9076	0.66	0.0503	2.12	0.2432	2.7	0.0358	0.66	0.25	161	61	227	2	221	6	0.97	227	2	1.622						
110609-2B-8	134	180	27.8562	1.18	0.0483	5.78	0.2392	5.9	0.0359	1.18	0.20	115	136	228	3	218	13	0.95	228	3	1.344						
110609-2B-7	65	117	27.3931	1.63	0.0510	6.35	0.2032	15.0	0.0360	1.75	0.12	-295	381	231	4	188	28	0.88	discordant	4							
110609-2B-1	35	57	27.5347	2.21	0.0458	7.27	0.1942	14.1	0.0360	2.27	0.16	-410	364	231	5	180	25	0.78	discordant	5							
110609-2B-6	57	46	27.4338	1.75	0.0509	5.86	0.1807	21.6	0.0358	1.96	0.09	-586	582	231	4	169	36	0.79	discordant	4							
Holbrook																											
103009-1G-3	378	462	29.1567	0.67	0.0507	2.14	0.2368	2.4	0.0343	0.67	0.28	200	54	217	1	216	5	0.99	217	1	1.222	224 ± 5 Ma	1.66				
103009-1G-9	144	233	28.8849	1.12	0.0525	3.50	0.2328	5.3	0.0345	1.14	0.21	147	122	219	2	212	11	0.97	219	2	1.612						
103009-1G-5	139	233	28.8115	1.13	0.0525	3.54	0.2318	6.5	0.0345	1.17	0.18	132	149	219	3	212	14	0.96	219	3	1.673						
103009-1G-8	244	603	28.7128	0.85	0.0512	2.68	0.2266	4.7	0.0347	0.88	0.19	70	110	221	2	207	10	0.94	221	2	2.469						
103009-1G-6	202	236	28.2377	0.94	0.0528	2.90	0.2377	5.1	0.0352	0.96	0.19	144	119	224	2	217	11	0.97	224	2	1.169						
103009-1G-2	542	1092	28.2790	0.56	0.0516	1.75	0.2433	2.4	0.0353	0.57	0.24	195	53	224	1	221	5	0.99	224	1	2.016						
103009-1G-10	139	96	28.1017	1.12	0.0507	3.54	0.2523	3.7	0.0356	1.12	0.30	258	82	225	3	228	9	1.01	225	3	0.691						
103009-1G-1	327	308	28.0258	0.73	0.0511	2.32	0.2417	3.4	0.0356	0.75	0.22	159	78	226	2	220	8	0.97	226	2	0.942						
103009-1G-11	426	1168	27.6499	0.65	0.0492	2.08	0.2420	2.3	0.0361	0.65	0.28	127	53	229	2	220	5	0.96	229	2	2.738						
103009-1G-12	101	206	27.3845	1.32	0.0526	4.08	0.2465	5.8	0.0364	1.33	0.23	156	131	231	3	224	13	0.97	231	3	2.045						
103009-1G-4	88	116	27.5636	1.38	0.0509	4.47	0.2116	10.3	0.0359	1.45	0.14	-183	255	230	3	195	20	0.85	discordant	3							
103009-1G-7	77	120	29.9533	1.48	0.0500	4.77	0.1818	12.9	0.0330	1.58	0.12	-351	331	212	3	170	22	0.80	discordant	3							

[§]Concordance determined by age(²⁰⁶Pb*/²³⁸U)/age(²⁰⁷Pb*/²³⁵U) for grains < 1000 Ma, and age(²⁰⁶Pb*/

The majority of grains are euhedral and have acicular habits, though some are barrel shaped. Although most zircons have well-preserved zoning bands, zoning patterns are commonly not apparent in rounded grains. Volcanic zircon grains are also euhedral, and in most cases zoning bands parallel crystal rims, although overgrowths are apparent in some cases.

Joseph City, Arizona (UTM Zone 12, 0565370, 3870314)

The Shinarump Member at Joseph City, Arizona, (Fig. 1; sample JCNEWs, Supplemental Table; samples JC, JCNEW, Table 2A) is medium- to coarse-grained sandstone with poorly to moderately indurated, matrix-supported conglomerate interbeds. Clasts are well-rounded, moderately sorted granules to cobbles of limestone, quartzite, and chert, with rare porphyritic volcanic clasts. Maximum clast size is 4–5 cm and volcanic clasts are ~2% of the total.

Cathodoluminescence imaging was not done on Joseph City detrital zircons, but zircon grains have a high percentage of euhedral, acicular forms. Fewer grains are rounded to barrel shaped. CL images from clast zircons are of very poor quality.

North Park, Arizona (UTM Zone 12, 0528073, 3885140)

The North Park, Arizona (Howell, 2010; Fig. 1; sample North Park, Supplemental Table), sample material is from matrix-supported, trough cross-stratified cobble conglomerate with sandstone lenses. The sample was collected dominantly from a coarse- to very coarse-grained subarkosic arenite, with a small portion taken from a fine- to medium-grained fraction at the same stratigraphic level. Clasts are limestone and quartzite and are generally 3–5 cm, with rare white volcanic clasts <3 cm in diameter. Zircons from the North Park sample were separated and analyzed as part of Howell's (2010) study and were not imaged.

Hunt, Arizona (UTM Zone 12, 0620522, 3836741)

Sandstone at Hunt, Arizona, has traditionally been assigned to the Mesa Redondo Member (Cooley, 1958) (Fig. 1; sample 050511-ss, Supplemental Table; samples 120309 and 050511, Table 2A). The sampled material is poorly to moderately indurated, coarse grained, and thin to medium bedded. Conglomerate interbeds and lenses are trough cross-bedded and 2–3 m thick and consist of matrix-supported, poorly to moderately sorted, well-rounded granules to cobbles of chert, quartzite, limestone, and ~1% porphyritic volcanic clasts that typically weather to a pitted texture. Maximum clast size is 4–5 cm.

Detrital zircons from the Hunt sample are approximately equal parts acicular, barrel shaped, and rounded. Many rounded grains do not have clear zoning bands. More rarely, subhedral grains have zone bands that are truncated along the grain margin. CL images of clast zircons show euhedral, concentric zoned grains.

ANALYTICAL METHODS

Zircons were extracted from sandstone by standard methods (e.g., Gehrels, 2000) with minimal magnetic separation (0.1–0.3 amperes). Zircons from the Hunt, Holbrook, Joseph City, Cedar Ranch, Paria, and Muddy Mountains sandstone samples underwent annealing and chemical abrasion (cf. Mattinson, 2005; Riggs et al., 2013). Cathodoluminescence imaging to identify cores was done at Northern Arizona University using a JSM-6480LV scanning electron microscope. Zircons from the North Park and Cameron samples are from Howell (2010) and were not annealed or chemically abraded before analysis at the University of Arizona LaserChron Center. All detrital zircon samples were analyzed for U and Pb isotopes and for trace element concentrations at the University of California–Santa Barbara (UCSB) Laser Ablation Split Stream (LASS) facility using a Nu Plasma HR MC-ICPMS (high resolution multi-collector–inductively coupled plasma mass spectrometer), a Nu AttoM single collector ICPMS (Nu Instruments Ltd., Wrexham, UK), and an Analyte 193 excimer ArF laser-ablation system equipped with a HeLex sample cell (Photon Machines, San Diego, USA) using a 24 μm beam. Analyses are normalized against the 91500 zircon standard as a reference material (1062 Ma; Wiedenbeck et al., 1995). Data were reduced using Lolite 2.31 software in Igor Pro 6.3. Error assessment follows Kylander-Clark et al. (2013).

Zircons from the Cameron site and a portion of the North Park sample analyzed at the University of Arizona LaserChron Center were ablated by a New Wave UP193HE Excimer laser (operating at a wavelength of 193 nm) using a spot diameter of 30 μm. All measurements were made in static mode, using a Nu Plasma HR MC-ICPMS and Faraday detectors with $3 \times 10^{11} \Omega$ resistors for ^{238}U , ^{232}Th , and ^{208}Pb – ^{206}Pb , and discrete dynode ion counters for ^{204}Pb and ^{202}Hg . Ion yields were ~0.8 mV per ppm. Each analysis consisted of one 15 s integration on peaks with the laser off (for backgrounds), fifteen 1 s integrations with the laser firing, and a 30 s delay to purge the previous sample and prepare for the next analysis. In this analysis mode, ablation pits are typically ~15 μm in depth. Uncertainties shown in Table 2B are at the 1σ level and include only measurement errors. Data were reduced using an in-house program.

Zircons were extracted from volcanic clasts by standard methods, but were not annealed or chemically abraded. A minimum of four zircons were analyzed from each clast reported on here.

Zircons from most volcanic cobbles were also analyzed in the UCSB LASS lab using methods described above. Isotope ratios and elemental concentrations in zircons from four clasts (Table 2B) were measured using the U.S. Geological Survey SHRIMP-RG at Stanford University (California, USA). Zircons were mounted in epoxy and imaged with a CL detector on a scanning electron microscope. These images were used to guide selection of analysis points. Zircons were ablated using a ~30-μm-diameter, 5–6 nA O₂ primary beam. For Th and U concentrations and Pb/U ratios, data reduction used SQUID (a Microsoft Excel add-in that yields reduced and corrected isotope ratios and ages from raw SHRIMP U-Th-Pb data [www.bgc.org/isoplot_etc/squid.html]) and Isoplot software (www.bgc.org/isoplot_etc/isoplot.html), and followed procedures

described in Barth and Wooden (2006). All ion microprobe zircon ages were standardized against Braintree Complex zircon R33 (419 Ma; Black et al., 2004); ages of individual analytical spots are reported at the 1σ level.

Detrital zircon analytical data are provided in the Supplemental Table, and all age errors reported are 2σ , unless stated otherwise. Analyses were evaluated for discordance based on a comparison of $^{235}\text{U}/^{207}\text{Pb}$ and $^{238}\text{U}/^{206}\text{Pb}$ for Permian and Triassic grains, and of $^{207}\text{Pb}/^{206}\text{Pb}$ and $^{238}\text{U}/^{206}\text{Pb}$ for Proterozoic grains. Grains that were $>10\%$ normally discordant (i.e., $^{235}\text{U}/^{207}\text{Pb}$ age $>10\%$ older than $^{238}\text{U}/^{206}\text{Pb}$ age) or $>5\%$ reversely discordant (i.e., $^{238}\text{U}/^{206}\text{Pb}$ age $>5\%$ older than $^{235}\text{U}/^{207}\text{Pb}$ age) were not used in interpretations; these are indicated by “discordant” in Table 1 and the Supplemental Table.

RESULTS

Twenty-three volcanic clasts in the Shinarump Formation each yielded between three and 29 grains with Triassic ages; clasts range in age from ca. 232 Ma to ca. 224 Ma (Tables 2A, 2B). All sampled locations contain clasts across this age range. Most clasts have a narrow range of spot ages, with error assigned by Isoplot's TuffZirc of 1–5 m.y. (Tables 2A, 2B); we take 2 m.y. as a best estimate of analytical error. Rare older grains are likely antecrysts, and in only one case (sample 110906-1D, Table 2B) does a grain lie below and outside the error bar of the grains that are included by Isoplot in a TuffZirc plot. We infer the date assigned by TuffZirc to be the best estimate of crystallization age for the individual clasts. No grouping of ages is apparent, although the range of 227–229 Ma is most strongly represented ($n = 13$). Th/U ratios, which provide information about magma chemistry and may be a powerful tool for understanding the relation between detrital materials and putative sources (e.g., Riggs et al., 2012, 2013; Barth et al., 2013), vary relatively little. Averaged Th/U values for individual clasts in general cluster between 0.9 and 1.7 (Table 1). It is also noteworthy that clasts from the Hunt site, which has been assigned to the Mesa Redondo Member, have identical clast ages and Th/U values to Shinarump Member clasts.

Overall, detrital zircon signatures of the Shinarump Member have strong similarities as well as differences across our sample area (Figs. 2 and 3). All samples have a distinctive Triassic population, although the youngest zircon ages vary between locations. Detrital zircons from sandstones at the Paria and North Park sites are noteworthy in the low percentage of Permo-Triassic grains (8% and 17%, respectively) compared to 34–53% at Cameron, Cedar Ranch, Holbrook, Hunt, Joseph City, and Muddy Mountains. All samples have ca. 1400 Ma grains, and ca. 1100 Ma and 1600 Ma populations are common in most samples (Figs. 2 and 3).

Age data are complemented by Th/U values (Fig. 4). The majority of Permo-Triassic grains have Th/U values between 0.3 and 2.2; very few grains have ratios lower than 0.1.

Detrital zircons have a much broader range of Triassic ages than volcanic zircons at all sites. At Hunt and Holbrook, zircon ages and Th/U values of clasts

and Triassic grains overlap significantly, although at Hunt several grains form an older cluster and at Holbrook the range is broader. The Joseph City plot of age versus Th/U shows an isolated cluster of grains that has no apparent relation to clasts and just one grain that overlaps the dominant clast age and narrow Th/U ratio (Fig. 5). The North Park and Paria samples have very few grains in the 235–220 Ma range.

DISCUSSION

Derivation of Grains and Clasts

Detrital zircon grains fall into several major age groups. Rare Archaean and earliest Paleoproterozoic (ca. 3250–2500 Ma) grains in the Holbrook, Joseph City, and Paria samples (1.5% of total grains) were likely derived from eroded older sedimentary strata and/or cratonal rocks in the mid-continent. Dickinson and Gehrels (2008) noted similar-age grains only in their samples from the upper Chinle Formation, and considered it likely that the younger river system lay in closer proximity to these sources. Alternatively, our samples may have come from lower-order drainages that did not contribute significantly to the lower Chinle Formation trunk system described by those authors.

Paleo- through Neoproterozoic grains (ca. 2100–900 Ma) are more than half the grains in several samples and 52% of total grains. Within this large grouping, populations that represent southwest Laurentian tectonic elements are common (Fig. 1). Grains were derived from arc terrains related to the Yavapai (ca. 1800–1700 Ma) and Mazatzal (1700–1600 Ma) provinces and A-type “anorogenic” granites that range in age from ca. 1500 to 1300 Ma (Whitmeyer and Karlstrom, 2007). Lastly, Grenville-age (i.e., 1300–950 Ma) zircons are as much as 45% of analyzed grains from some Shinarump samples. Although plutons of these ages are exposed across southwestern Laurentia, Proterozoic zircons may also have been derived from uplifted and eroded Pennsylvanian–Permian sedimentary and metasedimentary strata that were part of the arc basement. Zircon grains with Proterozoic ages are common in these strata throughout southwestern North America (e.g., Soreghan et al., 2002; Soreghan et al., 2007).

The derivation of some Paleozoic grains is more complex. In contrast to the findings of Dickinson and Gehrels (2008) in Chinle Formation strata farther to the east, very few ($<1\%$) Cambrian grains (540–500 Ma) are present in the samples analyzed here. Approximately 3% of grains lie in a poorly defined range from ca. 300 to ca. 450 Ma; zircons of this age were attributed by Dickinson and Gehrels (2008) to sources in the Ouachita orogen.

Permo-Triassic zircons make up 40% of all detrital grains. Understanding their source(s) requires review of current knowledge about the distribution Permo-Triassic magmatic rocks in southwestern, southern, and southeastern Laurentia. Dickinson and Gehrels (2008) noted that few arc-related grains were present in their samples, and inferred that grains <232 Ma were derived from

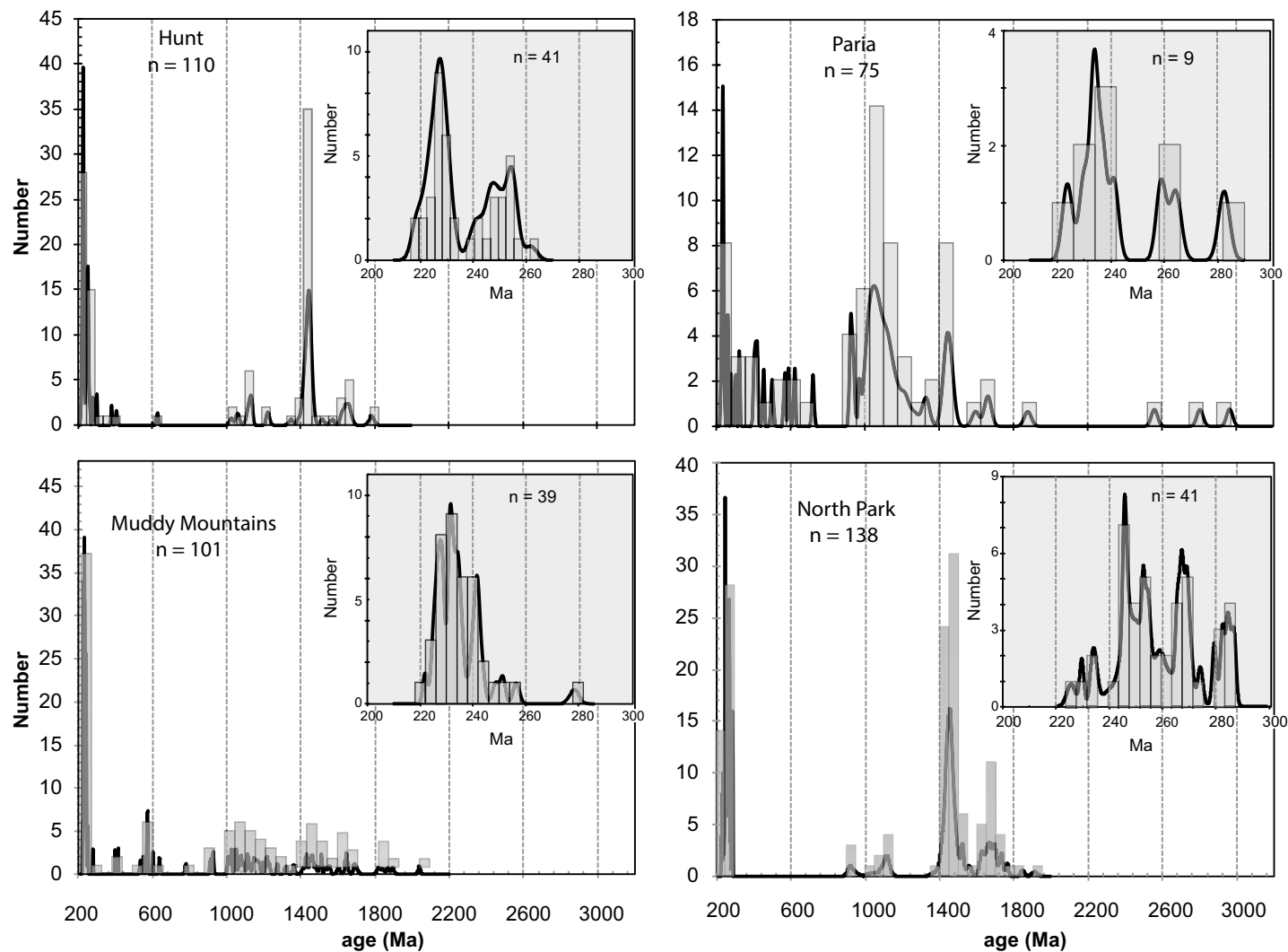


Figure 2 (on this and following page). Probability density plots for Shinarump conglomerate detrital zircon samples. Insets show Permian-Triassic grains only.

the Cordilleran arc, whereas those >245 Ma were derived from the “East Mexico” arc. The latter interpretation is supported by paleocurrents that dominantly indicate flow from the southeast. The few reliable dates that can be related to this arc, however, are from fine-grained lacustrine tuffs in the Quartermaster Formation and Dewey Lake Redbeds in west Texas that yield zircon ages of ca. 251 Ma (Fracasso and Kolker, 1985; Geissman et al., 2011). The source

of tuffs of the Quartermaster and Dewey Lake Formations is unknown, but the fine grain size supports a distant source, most likely to the west or to the southeast. The majority of magmatic rocks of the East Mexico arc are dated by K-Ar (Torres et al., 1999). One important exception is the Tuzancoa Formation in Hidalgo, eastern Mexico, in which fossiliferous volcanic and volcanoclastic rocks are dated by fossil evidence as Late Permian in age (Rosales-Lagarde

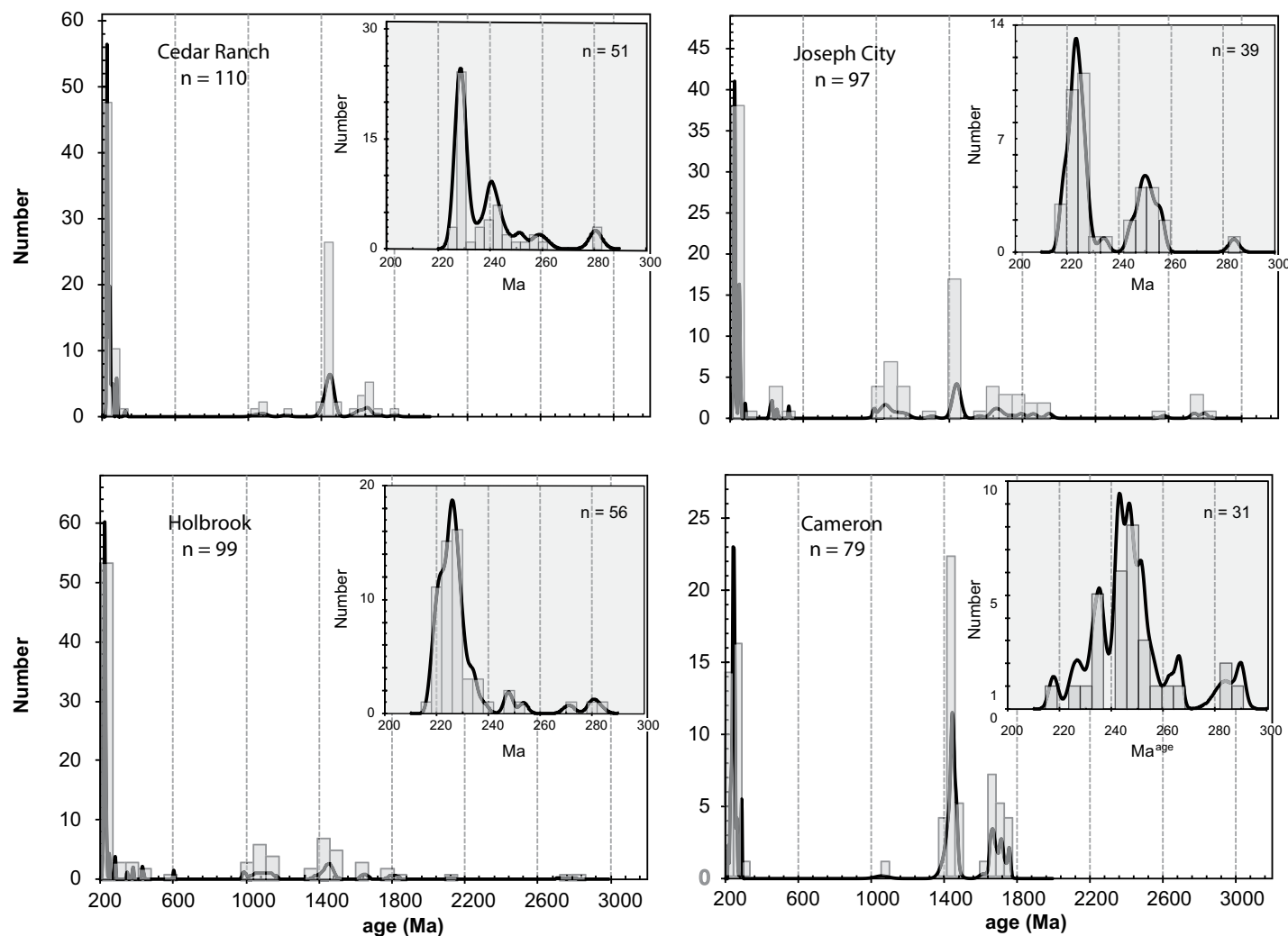


Figure 2 (continued).

et al., 2005). These rocks, however, are marine and exposed ~2000 km south of the Chinle depocenter, and thus are not a likely source. Likewise, the Totoltepec laccolith is dated by U-Pb as 289 ± 1 Ma (Keppie et al., 2004), but is much farther south than would be a likely source, as well as being an age that is very poorly represented in the Shinarump detrital population.

Cordilleran arc magmatism began by 270 Ma (Arvizu et al., 2009; Riggs et al., 2010), but detritus from that arc is present only locally in retro-arc sedi-

mentary strata older than Late Triassic (i.e., Lower Triassic Buckskin Formation; Sanchez et al., 2014). Preliminary results from Permian forearc rocks in Sonora, Mexico, indicate a strong influx of arc detritus at ca. 273 Ma (Riggs et al., 2014). The proximity of the Cordilleran arc, together with the growing body of information concerning its range of ages, makes it the most likely source region, thus requiring explanation of how the ages represented were mixed into the Shinarump depocenter.

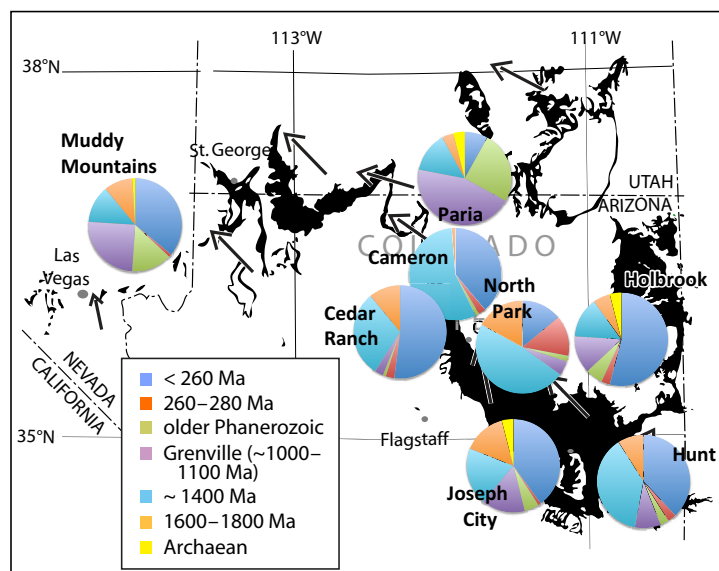


Figure 3. Pie plots demonstrating major detrital-zircon age similarities and differences between Chinle Formation sample sites. Chinle exposures are shown in black; arrows indicate paleocurrent directions. Little correlation exists between percentages of different-age zircons and position with respect to the Cordilleran arc.

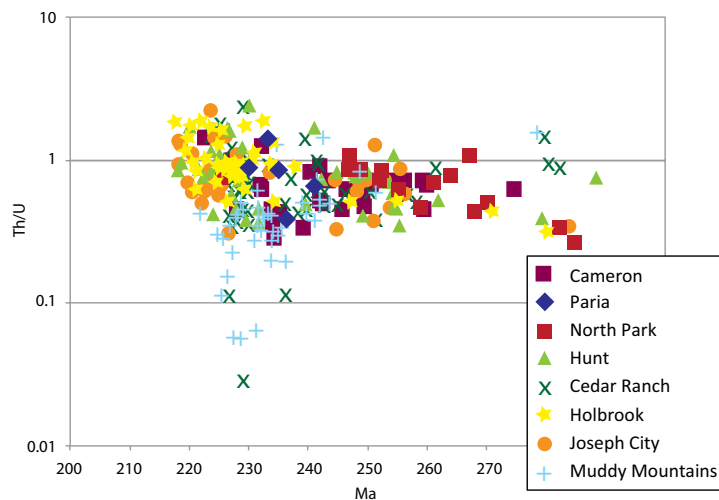


Figure 4. Th/U versus age plot for detrital grains.

The range of Permo-Triassic ages also bears examination, as dispersal paths must accommodate disparate areas that would have been sources. The oldest common Permian grains in our samples are ca. 280–285 Ma. These, together with ages to ca. 260 Ma, make up <5% of the total grains and are rare in all samples except North Park, and are inferred to derive from the Sonoran segment of the arc (Fig. 1).

The San Bernardino intrusive suite and plutons in the northern Mojave Desert (Fig. 1; Miller et al., 1995; Barth and Wooden, 2006) likely sourced ca. 260 and ca. 240 Ma grains in many of the samples. The correlation with the San Bernardino suite is suggested both by age and by similar Th/U ratios (Fig. 6). Data presented by Miller et al. (1995) do not include Th/U values; our preliminary results from these rocks show a reasonable overlap in Th/U values between 260–250 Ma grains in these plutons and in the detrital zircons in the Shinarump Member. Age and Th/U also support the derivation of ca. 235–230 Ma grains from the Granite Mountain suite (Fig. 1).

Many grains younger than ca. 230 Ma have less-certain sources. The intrusive suites documented by Barth and Wooden (2006) have only rare 230–220 Ma ages. Additionally, many detrital grains in this range have Th/U ratios higher than both older components of the sandstones and rocks of the intrusive suites (Fig. 6). Riggs et al. (2012) speculated that an as-yet-undocumented source for zircons in middle Chinle Formation sandstones is buried or has been eroded, but lay approximately in the Colorado River basin.

The breakdown of ages and potential source areas allows distinctions to be drawn between the sample sites, leading, in turn, to enhanced understanding of dispersal pathways; sites are discussed here from west to east. The Muddy Mountains (Fig. 1) site contains a group of zircons between ca. 240 and 243 Ma which match the San Bernardino suite in age and Th/U, grains between 230 and 236 Ma likely derived from the Granite Mountains suite, and grains between ca. 225 and 230 Ma that do not have an obvious source. Thus we infer that this area, which was close to the arc, either was fed by a stream system that tapped a relatively confined area within the arc or received detritus from Plinian ash columns. Proterozoic grains are well represented and were derived either from uplifted arc basement or from easterly sources. The lack of igneous clasts, however, is surprising considering the likely proximity to the arc. It should be reemphasized, however, that overall the percentage of volcanic clasts in any Shinarump conglomerate bed is generally very low (i.e., ≤5%), such that the clasts are more anomalous by their presence than absence.

The Cedar Ranch sample site contains two distinct groups of Permo-Triassic zircons. A diffuse cluster between ca. 237 and 240 Ma is consistent in age and Th/U ratios with derivation from the San Bernardino and/or Granite Mountain suites in the Mojave Desert. Zircon grains between ca. 230 and 225 Ma dominate the Permo-Triassic signature of this site. These grains overlap Mojave Desert plutons in age and Th/U to a lesser extent than the older grains, and are in part distinctive from similar-age grains in the Muddy Mountains sample. Thus we infer that some recycling of older grains may have occurred, but that the 230–225 Ma group reflects derivation from a specific part of the arc

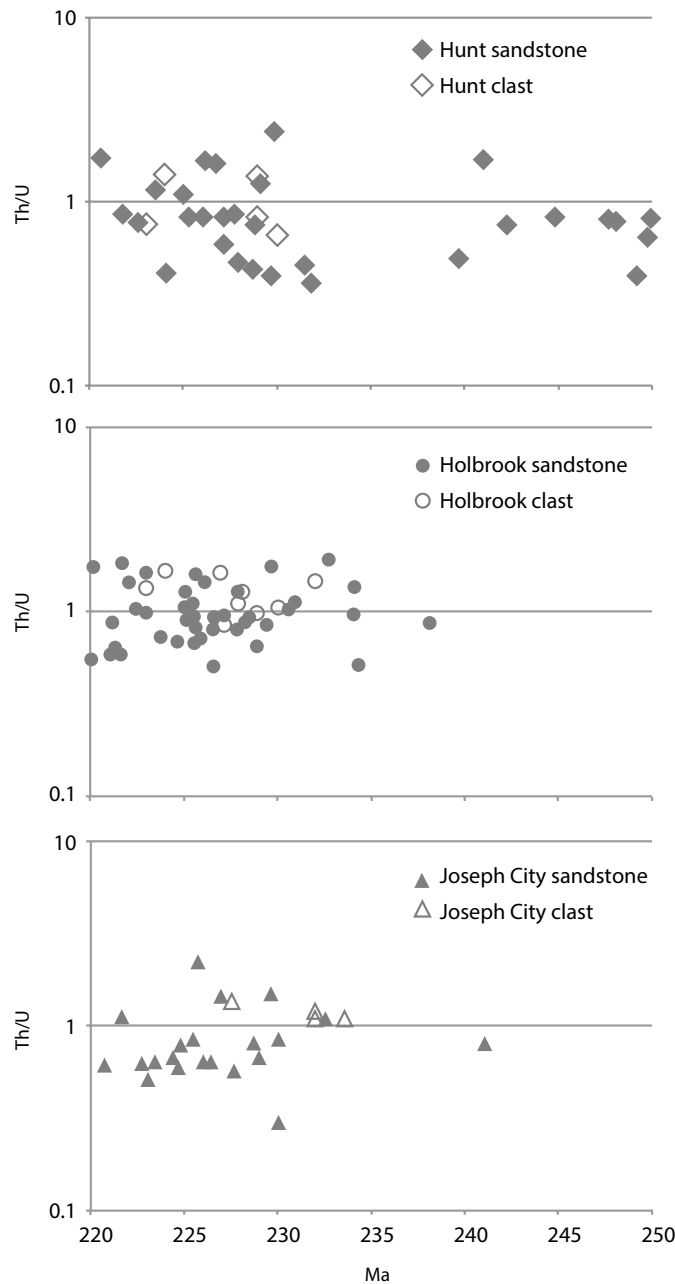


Figure 5. Th/U versus age plot for zircons in volcanic clasts from Hunt, Holbrook, and Joseph City compared with detrital zircons in sandstone from the same sample site. Cameron site is not shown because clasts and sandstone were not collected from the same location.

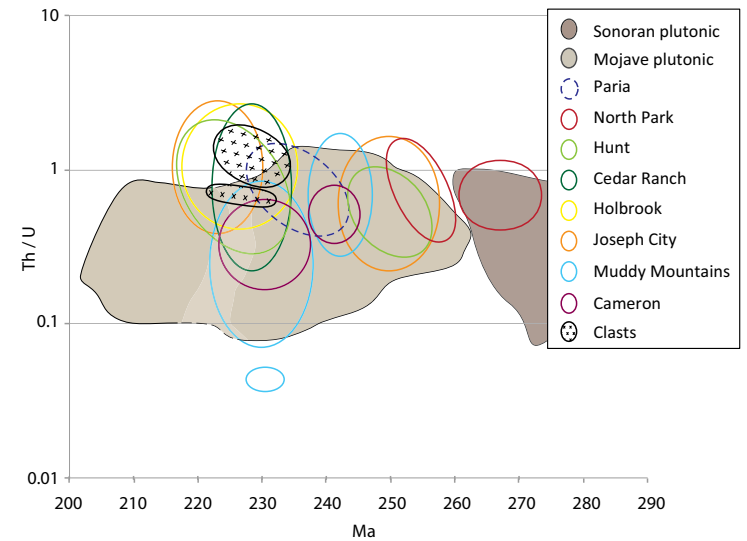


Figure 6. Comparison of age and Th/U for detrital zircons, clast zircons, and Triassic plutonic suites of southern and southeastern California. Pluton data from the Mojave Desert suites are from Barth and Wooden (2006). Dashed line for Paria is due to the very few Triassic zircons in that sample (n = 6). Lighter-color band within Mojave plutonic field is area of few zircon ages.

and that these grains were genetically related to volcanic clasts found in other samples (cf. Riggs et al., 2013).

The North Park sample is unique in its comparatively high percentage (13%) of Permian grains. Six of these grain lie in a discrete cluster from 288 to 282 Ma, and their source is uncertain. Zircons of this age are inferred by Dickinson and Gehrels (2008) to derive from the East Mexico arc; we question this interpretation for reasons provided above. On the western margin of Laurentia, however, transcurrent faulting was likely active at ca. 280 Ma, and subduction was established by ca. 270 Ma. Thus these grains are not considered likely to be derived from the Cordilleran margin. The majority of grain ages are in a comparatively narrow range, from ca. 270 to 247 Ma (n = 13); ages and Th/U are compatible with derivation from the Mojave Desert plutons and the Sonora portion of the arc (Fig. 6).

The youngest grains from the Holbrook, Hunt, and Joseph City samples are very similar in their age and chemistry; Hunt and Joseph City samples additionally have an older group of grains in the ca. 240–260 range Ma that were likely derived from the San Bernardino suite and/or older plutons in the northern Mojave Desert (Miller et al., 1995); Th/U ratios support correlation with both suites of plutons (Fig. 6). Grains as young as 218 Ma may have been subject to lead loss; on probability density plots the maxima are between 226 and 223 Ma (Fig. 4), and these older ages may be more suitable estimates

of the maximum depositional age. Th/U values are from within the range of the Granite Mountain suite to well above those values (Fig. 6). Clasts from all three sites, as well as those from Cameron, overlap the older part of the younger age range and have Th/U values that match higher detrital-grain values. We infer that these grains had a similar source to those from the Cedar Ranch site.

Grains that traveled from the Sonoran segment of the arc could reflect original deposition from ash clouds and strong dilution, or possibly longshore currents that brought detritus northward from the arc to be uplifted when detritus from the arc began to reach the continental landmass. Zircons that match plutons of the Mojave Desert in age and Th/U may have been carried by river systems or from ash clouds.

Paleotopography of the Early Mesozoic Arc

Our interpretation of the evolution of topography between the arc and retro-arc in Late Permian through Late Triassic time is by necessity constrained by a lack of detailed study of Late Permian rocks in southwest Laurentia. The southwest margin of Laurentia likely underwent induced subduction (cf. Gurnis et al., 2004; Stern, 2004; Saleeby, 2011) in Permian time as strike-slip faulting transitioned southward to subduction in northern Sonora, Mexico (Fig. 7; Arvizu et al., 2009; Riggs et al., 2010, 2014). Over time, Permian–Early Triassic magmatism became more widespread in California, forming an arc that lay offshore of the continental landmass. Very little detrital record remains of this time in equivalent-age strata, however, because the arc was marine and likely

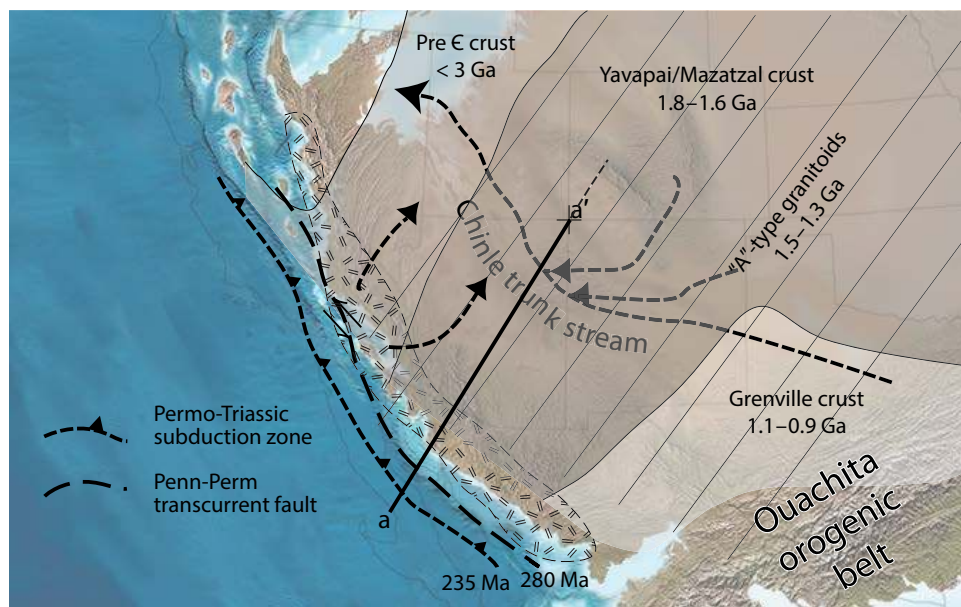
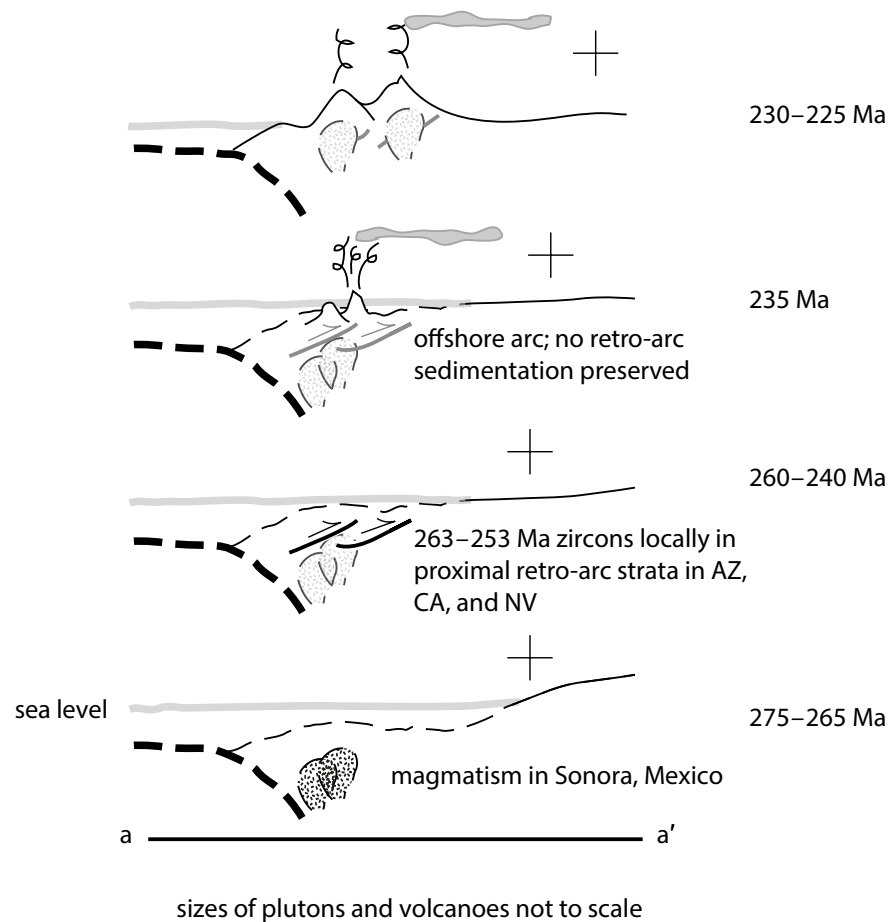


Figure 7. Summary tectonic reconstruction. Map shows schematic setting of Pennsylvanian–Permian strike-slip faulting along the Cordilleran margin and subduction initiation in Permian–Triassic time. Shaded areas are Proterozoic crustal provinces as for Figure 1 inset. Background paleotopographic reconstruction, copyright Ron Blakey, Colorado Plateau Geosystems, used with permission. Pre-C—Precambrian; AZ—Arizona; CA—California; NV—Nevada. For the full-sized version of Figure 7, please visit <http://dx.doi.org/10.1130/GES01238.S4> or the full-text article on www.gsapubs.org.



did not have substantial subaerial topography. The sedimentary record of the back-arc is confined to arc-proximal units such as the Buckskin Formation in eastern California and western Arizona, which in its lower members is equivalent to the Moenkopi Formation (Reynolds and Spencer, 1989) and which reflects magmatism at ca. 253 Ma (Sanchez et al., 2014), and in the southern Inyo Mountains in east-central California, where our data from the Lone Pine and Conglomerate Mesa Formations include prominent detrital zircon peaks at 263 and 257 Ma (Stevens et al., 2015; Riggs et al., 2015) (Fig. 7).

The date of 227.604 ± 0.082 Ma for the Mesa Redondo Member of the Chinle Formation, from a sample only a few meters above the contact with the Moenkopi Formation, supports initial deposition of the Chinle Formation at ca. 230 Ma, as suggested by Dickinson and Gehrels (2008), or 1–2 m.y. later. Between Early and Late Triassic time, arc magmatism in California transitioned to include volcanism. By this time, two major changes had occurred. First, a subaerial connection between arc and retro-arc was established that allowed fluvial transport of arc material to the Chinle basin (Fig. 7), perhaps by ca. 235 Ma. Second, because the record of volcanism is prominent as 230–225 Ma clasts, especially in younger conglomerates in the Chinle Formation, we infer that volcanic activity became common at this time, with eruption of intermediate to felsic lava and ignimbrite. Related Plinian ash clouds could have been a major source of fine-grained volcanic detritus. The observation that volcanic clasts are <5% of types in Shinarump conglomerate exposures suggests that the terrestrial connection between the marine arc and the continental landmass was limited in the earliest stages of Chinle deposition. Volcanic clasts are more common in the younger Sonsela Member, indicating that over time a subaerial fluvial connection became far more stable.

The Tr-3 unconformity separates Upper Triassic from Lower–Middle Triassic and older strata in western Laurentia (Stewart et al., 1972a; Pippingos and O’Sullivan, 1978). Howell and Blakey (2013) postulated that this surface represents response to dynamic subsidence of the Cordilleran arc, citing the similarity in trend between the erosional surface and the arc, and that development of the unconformity was driven by migration of the arc onto the continental margin. The youngest three-grain cluster in the Holbrook Sandstone Member of the Moenkopi Formation (Dickinson and Gehrels, 2008) yields an isoplot average age of 241 ± 2 Ma, which may provide an older age constraint on this event, and initiation of Shinarump Member sedimentation at ca. 230 Ma marks the latest time at which the arc would have become wholly subaerial. Howell and Blakey (2013) suggested that the on-shore migration of the arc occurred at ca. 235 Ma based on oldest Triassic detrital zircons in the Sonsela Member of the Chinle Formation; although our results show a much broader range of Permian–Triassic detrital grains in the older Shinarump Member, the ca. 235 Ma age is reasonable. In this case, erosion of underlying strata and development of the Tr-3 surface may have been a dramatic but relatively short-lived (i.e., 5–7 m.y.) event.

Processes that may have created a land connection between the arc and retro-arc region include crustal inflation due to emplacement of plutons, intra-arc tectonism and resultant uplift, and sea-level drop. Eustatic sea-level change

in Triassic time, however, is documented as predominantly transgressive (e.g., Hardenbol et al., 1998; Kelley et al., 2014), suggesting that isostatic forces (i.e., crustal inflation or uplift) dominated. Permo-Triassic intra-arc deformation is documented in the southwestern Mojave Desert and adjacent San Bernardino Mountains (Miller, 1981; Cameron, 1981; Miller and Cameron, 1982; Matti et al., 1993), as well as in the Red Cloud thrust system (Powell, 1981; Postlethwaite, 1988) and the Sierra Nevada–Death Valley thrust system (Snow, 1992; Stevens and Stone, 2005). Deformation is poorly dated in all of these systems, but evidence from cross-cutting plutons indicates at least some Permian–Triassic movement (Tosdal, 1988; Barth and Wooden, 2006; Stevens et al., 2015). These data indicate that regional intra-arc and proximal retro-arc uplift and exhumation were likely occurring by earliest Triassic time and that arc basement exhumation probably continued until earliest Jurassic time (Fig. 7). Crustal inflation may occur in and beneath volcanic arcs due to several mechanisms (see Chin et al. [2012] for a review); Chin et al. (2012) used xenolith compositional evolution to interpret crustal thickening below the Cretaceous Cordilleran arc, but similar data are not available for the earlier manifestations of the arc, and it is unlikely that the volume of magma input was sufficient to drive substantial thickening. Thus, although we would not discount crustal thickening as a process to bring the arc and nearby land above sea level, intra-arc deformation may have held the more important role.

CONCLUSIONS

New zircon data from sedimentary rocks and enclosed volcanic clasts from the Shinarump conglomerate in Arizona, southern Utah, and southeast Nevada provide insight into paleotopography of the growing Cordilleran arc and the nature of arc volcanism. The Shinarump conglomerate is the oldest retro-arc unit to contain volcanic clasts as well as fine-grained detritus, and thus yields the most complete data set regarding retro-arc sedimentation and the erosion of the arc. Volcanic clasts are ignimbrite and silicic lava, indicating that the arc erupted material from differentiated magmas and likely included stratovolcanoes and calderas. The 232–223 Ma ages of these clasts suggest derivation from a relatively confined area of the arc, in contrast to detrital grains, which have ages that span the known timing of arc plutonism (e.g., Miller et al., 1995; Barth and Wooden, 2006).

Analysis of Th/U values highlights the similarities and differences between inter- and intra-sample detrital grains and between detrital grains and clasts. Many of the detrital grains have Th/U values similar to those for Triassic Cordilleran arc plutons, and the combination of age and Th/U similarities strongly suggests derivation from those areas. Other grains, together with all of the clasts, have ages between ca. 230 and 225 Ma and Th/U values >1 that do not correspond to known Triassic Cordilleran plutonic rocks. These ages and Th/U values are similar to those in clasts and grain zircons from the Sonsela Member, higher in the Chinle Formation described by Riggs et al. (2012), and supports the speculation of those authors that material was derived from an

undocumented source in the Colorado River trough where continental crust was thicker and provided a higher Th signature.

Arc activity along western Laurentia began at ca. 275 Ma (Arvizu et al., 2009; Riggs et al., 2010; Lindner et al., 2012), but the oldest detrital zircon record of this arc is in sedimentary strata some 40 m.y. younger, suggesting that the arc developed offshore. Early Permian plutonism and volcanism in Sonora, Mexico, was dominantly or entirely subaqueous. Magmatism became more widespread during Late Permian and Early Triassic time, and eruptions may have breached the air-water interface. Ultimately, volcanic edifices became common in Late Triassic time, potentially synchronous with intra-arc deformation, which had the effect of bringing the arc above water and establishing a land bridge between arc and continent at ca. 230 Ma. At this point, erosion of the growing arc began to be seen in retro-arc fluvial strata of the Chinle Formation, ushering in continental sedimentation that has dominantly characterized the region since that time.

ACKNOWLEDGMENTS

Funding for this study was provided by the National Science Foundation through grant EAR-0711541 to Riggs. We are indebted to many colleagues whose discussions and studies have strongly informed our interpretations: R. Blakey, W. Dickinson, T. Lawton, S. Nesbitt, S. Reynolds, and S. Richard. Great thanks to C. Brailo for mineral-separation work, A. Kylander-Clark at UCSB for help in the LASS lab, the Tiffney-Gowan family for their hospitality, and E. Cullen for advice in drafting. Riggs also thanks Q. Crowley and B. Kamber at Trinity College Dublin (Ireland) for support during the sabbatical year. Reviews by Lynn Soreghan and Paul Stone were very helpful in identifying and clarifying murky ideas and writing, and are much appreciated.

REFERENCES CITED

- Akers, J.P., 1964, Geology and ground water in the central part of Apache County, Arizona: U.S. Geological Survey Water-Supply Paper 1771, 107 p.
- Arvizu, H.E., Iriondo, A., Izaguirre, A., Chávez-Cabello, G., Kamenov, G.D., Solís-Pichardo, G., Foster, D.A., and Lozano-Santa Cruz, R., 2009, Rocas graníticas pérmicas en la Sierra Pintada, NW de Sonora, México: Magmatismo de subducción asociado al inicio del margen continental activo del SW de Norteamérica: *Revista Mexicana de Ciencias Geológicas*, v. 26, p. 709–728.
- Atchley, S.C., Nordt, L.C., Sworin, S.I., Ramezani, J., Parker, W.G., Ash, S.R., and Bowring, S.A., 2013, A linkage among Pangean tectonism, cyclic alluviation, climate change, and biologic turnover in the Late Triassic: The record from the Chinle Formation, southwestern United States: *Journal of Sedimentary Research*, v. 83, p. 1147–1161, doi:10.2110/jsr.2013.89.
- Barth, A.P., and Wooden, J.L., 2006, Timing of magmatism following initial convergence at a passive margin, southwestern U.S. Cordillera, and ages of lower crustal magma sources: *The Journal of Geology*, v. 114, p. 231–245, doi:10.1086/499573.
- Barth, A.P., Walker, J.D., Wooden, J.L., Riggs, N.R., and Schweickert, R.A., 2011, Birth of the Sierra Nevada magmatic arc: Early Mesozoic plutonism and volcanism in the east-central Sierra Nevada of California: *Geosphere*, v. 7, p. 877–897, doi:10.1130/GES00661.1.
- Barth, A.P., Wooden, J.L., Jacobson, C.E., and Economos, R.C., 2013, Detrital zircon as a proxy for tracking the magmatic arc system: The California arc example: *Geology*, v. 41, p. 223–226, doi:10.1130/G33619.1.
- Basdekas, P., 1993, Provenance and diagenesis of the Shinarump Member, Triassic Chinle Formation, southern Nevada to southern Utah [M.S. thesis]: Flagstaff, Northern Arizona University, 142 p.
- Bateman, P.C., 1992, Plutonism in the central part of the Sierra Nevada batholith, California: U.S. Geological Survey Professional Paper 1483, 186 p.
- Black, L.P., Kamo, S.L., Allen, C.M., Davis, D.W., Aleinikoff, J.N., Valley, J.W., Mundil, R., Campbell, I.H., Korsch, R.J., Williams, I.S., and Foudoulis, C., 2004, Improved $^{206}\text{Pb}/^{238}\text{U}$ micro-

- probe geochronology by the monitoring of a trace-element-related matrix effect; SHRIMP, ID-TIMS, ELA-ICP-MS and oxygen isotope documentation for a series of zircon standards: *Chemical Geology*, v. 205, p. 115–140, doi:10.1016/j.chemgeo.2004.01.003.
- Blakey, R.C., and Gubitosa, R., 1983, Late Triassic paleogeography and depositional history of the Chinle Formation, southern Utah and northern Arizona, in Reynolds, M.W., and Dolly, E.D., eds., *Mesozoic Paleogeography of the West-Central United States: Rocky Mountain Section, Society of Economic Paleontologists and Mineralogists, Rocky Mountain Paleogeography Symposium 2*, p. 57–76.
- Cameron, C.S., 1981, Geology of the Sugarloaf and Delamar Mountain areas, San Bernardino Mountains, California [Ph.D. thesis]: Cambridge, Massachusetts Institute of Technology, 399 p.
- Camp, C.L., 1930, A study of the phytosaurs, with description of new material from western North America: *Memoirs of the University of California* 10, 174 p.
- Carr, M.D., Christiansen, R.L., Poole, F.G., and Goodge, J.W., 1997, Bedrock geologic map of the El Paso Mountains in the Garlock and El Paso Peaks 7–1/2' quadrangles, Kern County, California: U.S. Geological Survey Miscellaneous Investigations Series Map I-2389, 9 p., scale 1:24,000.
- Chin, E.J., Lee, C.A., Luffi, P., and Tice, M., 2012, Deep lithospheric thickening and refertilization beneath continental arcs: Case study of the *P*, *T* and compositional evolution of peridotite xenoliths from the Sierra Nevada, California: *Journal of Petrology*, v. 53, p. 477–511, doi:10.1093/ptrology/egr069.
- Colbert, E.H., and Gregory, J.T., 1957, Correlation of continental Triassic sediments by vertebrate fossils: *Geological Society of America Bulletin*, v. 68, p. 1456–1467.
- Cooley, M.E., 1958, The Mesa Redondo Member of the Chinle Formation, Apache and Navajo Counties, Arizona: *Plateau*, v. 31, no. 1, p. 7–15.
- Dickinson, W.R., and Gehrels, G.E., 2008, U-Pb ages of detrital zircons in relation to paleogeography: Triassic paleodrainage networks and sediment dispersal across southwest Laurentia: *Journal of Sedimentary Research*, v. 78, p. 745–764, doi:10.2110/jsr.2008.088.
- Dickinson, W.R., and Lawton, T.F., 2001, Carboniferous to Cretaceous assembly and fragmentation of Mexico: *Geological Society of America Bulletin*, v. 113, p. 1142–1160, doi:10.1130/0016-7606(2001)113<1142:CTCAAF>2.0.CO;2.
- Dodge, C.N., 1973, Pebbles from the Chinle and Morrison Formations, in James, H.L., ed., *Monument Valley and Vicinity, Arizona and Utah: New Mexico Geological Society Fall Field Conference Guidebook 24*, p. 114–121.
- Dubiel, R.F., 1987, Sedimentology of the Upper Triassic Chinle Formation, southeastern Utah [Ph.D. thesis]: Boulder, University of Colorado, 217 p.
- Dubiel, R.F., 1991, Architectural-facies analysis of nonmarine depositional systems in the Upper Triassic Chinle Formation, southeastern Utah, in Miall, A.D., and Tyler, N., eds., *The Three-Dimensional Facies Architecture of Terrigenous Clastic Sediments and Its Implications for Hydrocarbon Discovery and Recovery: SEPM (Society for Sedimentary Geology) Concepts in Sedimentology and Paleontology 3*, p. 103–110.
- Dubiel, R.F., and Hasiotis, S.T., 2011, Depositions, paleosols, and climatic variability in a continental system: The Upper Triassic Chinle Formation, Colorado Plateau, U.S.A., in Davidson, S.K., Leleu, S., and North, C.P., eds., *From River to Rock Record: The Preservation of Fluvial Sediments and their Subsequent Interpretation: SEPM (Society for Sedimentary Geology) Special Publication 97*, p. 393–421.
- Fisher, M.J., and Dunay, R.E., 1984, Palynology of the Petrified Forest Member of the Chinle Formation (Upper Triassic), Arizona, USA: *Pollen et Spores*, v. 26, p. 241–284.
- Fracasso, M.A., and Kolker, A., 1985, Late Permian volcanic ash beds in the Quartermaster–Dewey Lake formations, Texas Panhandle: *West Texas Geological Society Bulletin*, v. 24, no. 6, p. 5–10.
- Gehrels, G.E., 2000, Introduction to detrital zircon studies of Paleozoic and Triassic strata in western Nevada and northern California, in Soreghan, M.J., and Gehrels, G.E., eds., *Paleozoic and Triassic Paleogeography and Tectonics of Western Nevada and Northern California: Geological Society of America Special Paper 347*, p. 1–17, doi:10.1130/0-8137-2347-7.1.
- Geissman, J.W., Renne, P.R., Tabor, N.J., Mundil, R., Mitchell, W.S., III, Chang, Su-Chin, and Mack, G.H., 2011, “Ochoan” Quartermaster Formation of north Texas, USA, Part II: Magnetostratigraphy and geochronology: *Geological Society of America Abstracts with Programs*, v. 43, no. 5, p. 383.
- González-León, C., 1997, Sequence stratigraphy and paleogeographic setting of the Antimonio Formation (Late Permian–Early Jurassic), Sonora, Mexico: *Revista Mexicana de Ciencias Geológicas*, v. 14, p. 136–148.

- González-León, C.M., Stanley, G.D., Jr., Gehrels, G.E., and Centeno-García, E., 2005, New data on the lithostratigraphy, detrital zircon and Nd isotope provenance, and paleogeographic setting of the El Antimonio Group, Sonora, Mexico, *in* Anderson, T.H., Nourse, J.A., McKee, J.W., and Steiner, M.B., eds., *The Mojave-Sonora Megashear Hypothesis: Development, Assessment, and Alternatives: Geological Society of America Special Paper 393*, p. 259–282, doi:10.1130/0-8137-2393-0-259.
- Gurnis, M., Hall, C., and Lavier, L., 2004, Evolving force balance during incipient subduction: *Geochemistry Geophysics Geosystems*, v. 5, Q07001, doi:10.1029/2003GC000681.
- Hardenbol, J., Thierry, J., Farley, M.B., Jacquin, T., de Graciansky, P.-C., and Vail, P.R., 1998, Mesozoic and Cenozoic sequence chronostratigraphic framework of European basins, *in* de Graciansky, P.-C., Hardenbol, J., Jacquin, T., and Vail, P.R., eds., *Mesozoic and Cenozoic Sequence Stratigraphy of European Basins: SEPM (Society for Sedimentary Geology) Special Publication 60*, p. 3–14, doi:10.2110/pec.98.02.0003.
- Harshbarger, J.W., Repenning, C.A., and Irwin, J.H., 1957, Stratigraphy of the uppermost Triassic and Jurassic rocks of the Navajo country (Colorado Plateau): U.S. Geological Survey Professional Paper 291, 74 p.
- Howell, E.R., 2010, Depositional history of the Sonsela Member, Upper Triassic Chinle Formation, Petrified Forest National Park, Arizona [M.S. thesis]: Flagstaff, Northern Arizona University, 233 p.
- Howell, E.R., and Blakey, R.C., 2013, Sedimentological constraints on the evolution of the Cordilleran arc: New insights from the Sonsela Member, Upper Triassic Chinle Formation, Petrified Forest National Park (Arizona, USA): *Geological Society of America Bulletin*, v. 125, p. 1349–1368, doi:10.1130/B30714.1.
- Irmis, R.B., Mundil, R., Martz, J.W., and Parker, W.G., 2011, High-resolution U-Pb ages from the Upper Triassic Chinle Formation (New Mexico, USA) support a diachronous rise of dinosaurs: *Earth and Planetary Science Letters*, v. 309, p. 258–267, doi:10.1016/j.epsl.2011.07.015.
- Jaffey, A.H., Flynn, K.F., Glenenin, L.E., Bently, W.C., and Essling, A.M., 1971, Precision measurement of the half-lives and specific activities ^{235}U and ^{238}U : *Phys. Rev., Ser. C* 4, p. 1889–1906.
- Kelley, N.P., Motani, R., Jiang, D., Rieppel, O., and Schmitz, L., 2014, Selective extinction of Triassic marine reptiles during long-term sea-level changes illuminated by seawater strontium isotopes: *Palaeogeography, Palaeoclimatology, Palaeoecology*, v. 400, p. 9–16, doi:10.1016/j.palaeo.2012.07.026.
- Keppie, J.D., Nance, R.D., Dostal, J., Ortega-Rivera, A., Brent, V.M., Fox, D., Muise, J., Powell, J.T., Mumma, S.A., and Lee, J.W.K., 2004, Mid-Jurassic tectonothermal event superposed on a Paleozoic geological record in the Acatlán Complex of southern Mexico: Hotspot activity during the breakup of Pangea: *Gondwana Research*, v. 7, p. 238–260, doi:10.1016/S1342-937X(05)70323-3.
- Kylander-Clark, A.R.C., Hacker, B.R., and Cottle, J.M., 2013, Laser-ablation split-stream ICP petrochronology: *Chemical Geology*, v. 345, p. 99–112, doi:10.1016/j.chemgeo.2013.02.019.
- Lawton, T.F., 1994, Tectonic setting of Mesozoic sedimentary basins, Rocky Mountain region, United States, *in* Caputo, M.V., et al., eds., *Mesozoic Systems of the Rocky Mountain Region, USA: Denver, Colorado, Rocky Mountain Section, SEPM (Society for Sedimentary Geology)*, p. 1–25.
- Lindner, P.J., Riggs, N.R., and González-León, C., 2012, Provenance study of latest Paleozoic to Mesozoic El Antimonio Group, Sonora, Mexico, and implications for tectonic evolution of southwest Laurentia: *Geological Society of America Abstracts with Programs*, v. 44, no. 3, p. 11.
- Lucas, S.G., and Hunt, A.P., 1993, Tetrapod biochronology of the Chinle Group (Upper Triassic), western United States: *New Mexico Museum of Natural History and Science Bulletin*, v. 3, p. 327–329.
- Lupe, R., and Silberling, N.J., 1985, Genetic relationships between lower Mesozoic continental strata of the Colorado Plateau and marine strata of the western Great Basin: Significance for accretionary history of Cordilleran lithotectonic terranes, *in* Howell, D.G., ed., *Tectonostratigraphic Terranes of the Circum-Pacific Region: Circum-Pacific Council for Energy and Mineral Resources Earth Science Series 1*, p. 263–271.
- Martin, M.W., and Walker, J.D., 1995, Stratigraphy and paleogeographic significance of metamorphic rocks in the Shadow Mountains, western Mojave Desert, California: *Geological Society of America Bulletin*, v. 107, p. 354–366, doi:10.1130/0016-7606(1995)107<0354:SAPSOM>2.3.CO;2.
- Matti, J.C., Brown, H.J., Miller, F.K., Wrucke, C.T., Calzia, J.P., and Conway, C.M., 1993, Preliminary geologic map of the north-central San Bernardino Mountains, California: U.S. Geological Survey Open File Report 93-544, 9 p.
- Mattinson, J.M., 2005, Zircon U–Pb chemical abrasion (“CA-TIMS”) method: Combined annealing and multi-step partial dissolution analysis for improved precision and accuracy of zircon ages: *Chemical Geology*, v. 220, p. 47–66, doi:10.1016/j.chemgeo.2005.03.011.
- Miller, E.L., 1981, Geology of the Victorville region, California: *Geological Society of America Bulletin*, v. 92, part II, p. 554–608, doi:10.1130/GSAB-P2-92-554.
- Miller, E.L., and Cameron, C.S., 1982, Late Precambrian to Late Cretaceous evolution of the southwestern Mojave Desert, California, *in* Cooper, J.D., compiler, *Geology of Selected Areas in the San Bernardino Mountains, Western Mojave Desert, and Southern Great Basin, California: Shoshone, California, Death Valley Publishing*, p. 21–34.
- Miller, E.L., Miller, M.M., Stevens, C.H., Wright, J.E., and Madrid, R., 1992, Late Paleozoic paleogeographic and tectonic evolution of the western U.S. Cordillera, *in* Burchfiel, B.C., Lipman, P.W., and Zoback, M.L., eds., *The Cordilleran Orogen: Conterminous U.S.: Boulder, Colorado, Geological Society of America, Geology of North America*, v. G-3, p. 57–106.
- Miller, J.S., Glazner, A.F., Walker, J.D., and Martin, M.W., 1995, Geochronologic and isotopic evidence for Triassic–Jurassic emplacement of the eugeoclinal allochthon in the Mojave Desert region, California: *Geological Society of America Bulletin*, v. 107, p. 1441–1457, doi:10.1130/0016-7606(1995)107<1441:GAIEFT>2.3.CO;2.
- Oberling, Z.A., 2015, Petrogenesis and provenance of volcanic clasts in the Upper Triassic Shinarump Member, Chinle Formation, and equivalents: Implications for Early Triassic Cordilleran arc magmatism [M.S. thesis]: Flagstaff, Northern Arizona University, 262 p.
- Oberling, Z.A., Riggs, N.R., Barth, A.P., and Walker, J.D., 2010, Major and trace element geochemistry and $^{87}\text{Sr}/^{86}\text{Sr}$ and ϵNd isotopic compositions of volcanic clasts from the Shinarump Member, Upper Triassic Chinle Formation: *Geological Society of America Abstracts with Programs*, v. 42, no. 5, p. 646.
- Pipiringos, G.N., and O’Sullivan, R.B., 1978, Principal unconformities in Triassic and Jurassic rocks, western interior United States: A preliminary survey: U.S. Geological Survey Professional Paper 1035-A, 29 p.
- Postlethwaite, C.E., 1988, The structural geology of the Red Cloud thrust system, southern Eastern Transverse Ranges, California [Ph.D. thesis]: Ames, Iowa State University, 135 p.
- Powell, R.E., 1981, Geology of the crystalline basement complex, Eastern Transverse Ranges, southern California [Ph.D. thesis]: Pasadena, California Institute of Technology, 441 p.
- Rains, J.R., Marsaglia, K.M., and Dunne, G.C., 2012, Stratigraphic record of subduction initiation in the Permian metasedimentary succession of the El Paso Mountains, California: *Lithosphere*, v. 4, p. 533–552, doi:10.1130/L165.1.
- Ramezani, J., Hoke, G.D., Fastovsky, D.E., Bowring, S.A., Therrien, F., Dworkin, S.I., Atchley, S.C., and Nordt, L.C., 2011, High-precision U–Pb zircon geochronology of the Late Triassic Chinle Formation, Petrified Forest National Park (Arizona, USA): Temporal constraints on the early evolution of dinosaurs: *Geological Society of America Bulletin*, v. 123, p. 2142–2159, doi:10.1130/B30433.1.
- Ramezani, J., Fastovsky, D.E., and Bowring, S.A., 2014, Revised chronostratigraphy of the lower Chinle Formation strata in Arizona and New Mexico (USA): High-precision U–Pb geochronological constraints on the Late Triassic evolution of dinosaurs: *American Journal of Science*, v. 314, p. 981–1008, doi:10.2475/06.2014.01.
- Reif, D.S., and Slatt, R.M., 1979, Red bed members of the Lower Triassic Moenkopi Formation, southern Nevada: Sedimentology and paleogeography of a muddy tidal flat deposit: *Journal of Sedimentary Petrology*, v. 49, p. 869–890.
- Reynolds, S.J., and Spencer, J.E., 1989, Pre-Tertiary rocks and structures in the upper plate of the Buckskin detachment fault, west-central Arizona, *in* Spencer, J.E., and Reynolds, S.J., eds, *Geology and Mineral Resources of the Buckskin and Rawhide Mountains, West-Central Arizona: Arizona Geological Survey Bulletin 198*.
- Reynolds, S.J., Spencer, J.E., Asmerom, Y., DeWitt, E., and Laubach, S.E., 1989, Early Mesozoic uplift in west-central Arizona and eastern California: *Geology*, v. 17, p. 207–211, doi:10.1130/0091-7613(1989)017<0207:EMUIWC>2.3.CO;2.
- Riggs, N.R., Ash, S.R., Barth, A.P., Gehrels, G.E., and Wooden, J.L., 2003, Isotopic age of the Black Forest Bed, Petrified Forest Member, Chinle Formation, Arizona: An example of dating a continental sandstone: *Geological Society of America Bulletin*, v. 115, p. 1315–1323, doi:10.1130/B25254.1.
- Riggs, N.R., Barth, A.P., Wooden, J.L., and Walker, J.D., 2010, Use of zircon geochemistry to tie volcanic detritus to source plutonic rocks: An example from Permian northwestern Sonora, Mexico: *Geological Society of America Abstracts with Programs*, v. 42, no. 5, p. 267.
- Riggs, N.R., Barth, A.P., González-León, C., Jacobson, C.E., Howell, E., Wooden, J.E., and Walker, J.D., 2012, Provenance of Upper Triassic strata in southwestern North America as suggested by isotopic analysis and chemistry of zircon crystals, *in* Rasbury, E.T., Hemming, S., and Riggs, N., eds., *Mineralogical and Geochemical Approaches to Provenance: Geological Society of America Special Paper 487*, p. 13–36, doi:10.1130/2012.2487(02).

- Riggs, N.R., Reynolds, S.J., Lindner, P.J., Howell, E.R., Barth, A.P., Parker, W.G., and Walker, J.D., 2013, The Early Mesozoic Cordilleran arc and Late Triassic paleotopography: The detrital record in upper Triassic sedimentary successions on and off the Colorado Plateau: *Geosphere*, v. 9, p. 602–646, doi:10.1130/GES00860.1.
- Riggs, N.R., González-León, C.M., Cecil, M.R., Marsaglia, K., and Navas-Parejo, P., 2014, Age of the Permian Monos Formation, northern Sonora, Mexico, and implications for initiation of the Cordilleran magmatic arc: *Geological Society of America Abstracts with Programs*, v. 46, no. 6, p. 377.
- Riggs, N.R., Cecil, M.R., Stone, P.A., Stevens, C.H., and Sanchez, T.B., 2015, Permian arc magmatism and its detrital record in southwest Laurentia: *Geological Society of America Abstracts with Programs*, v. 47, no. 7, p. 262.
- Rosales-Lagarde, L., Centeno-García, E., Dostal, J., Sour-Tovar, F., Ochoa-Camarillo, H., and Quiroz-Barroso, S., 2005, The Tuzanco Formation: Evidence of an Early Permian submarine continental arc in east-central Mexico: *International Geology Review*, v. 47, p. 901–919, doi:10.2747/0020-6814.47.9.901.
- Saleeby, J., 2011, Geochemical mapping of the Kings-Kaweah ophiolite belt, California: Evidence for progressive mélange formation in a large offset transform-subduction initiation environment, in Wakabayashi, J. and Dilek, Y., eds., *Mélanges: Processes of Formation and Societal Significance*: Geological Society of America Special Paper 480, p. 31–73, doi:10.1130/2011.2480(02).
- Saleeby, J.B., Busby-Spera, C., Oldow, J.S., Dunne, G.C., Wright, J.E., Cowan, D.S., Walker, N.W., and Allmendinger, R.W., 1992, Early Mesozoic tectonic evolution of the western U.S. Cordillera, in Burchfiel, B.C., Lipman, P.W., and Zoback, M.L., eds., *The Cordilleran Orogen: Conterminous U.S.: Boulder, Colorado*, Geological Society of America, *Geology of North America*, v. G-3, p. 107–168.
- Sanchez, T.B., Riggs, N.R., Reynolds, S.J., and Barth, A.P., 2014, Early Mesozoic Cordilleran arc magmatism: The detrital zircon record of the Buckskin Formation, west-central Arizona and southeastern California: *Geological Society of America Abstracts with Programs*, v. 46, no. 6, p. 441.
- Snow, J.K., 1992, Large-magnitude Permian shortening and continental-margin tectonics in the southern Cordillera: *Geological Society of America Bulletin*, v. 104, p. 80–105, doi:10.1130/0016-7606(1992)104<0080:LMPSAC>2.3.CO;2.
- Soreghan, G.S., Moses, A.M., Soreghan, M.J., Hamilton, M., Fanning, C.M., and Link, P.K., 2007, Palaeoclimatic inferences from upper Palaeozoic siltstone of the Earp Formation and equivalents, Arizona–New Mexico (USA): *Sedimentology*, v. 54, p. 701–719, doi:10.1111/j.1365-3091.2007.00857.x.
- Soreghan, M.J., Soreghan, G.S., and Hamilton, M.A., 2002, Paleowinds inferred from detrital-zircon geochronology of upper Paleozoic loessite, western equatorial Pangea: *Geology*, v. 30, p. 695–698, doi:10.1130/0091-7613(2002)030<0695:PIFDZG>2.0.CO;2.
- Stern, R.J., 2004, Subduction initiation: Spontaneous and induced: *Earth and Planetary Science Letters*, v. 226, p. 275–292, doi:10.1016/S0012-821X(04)00498-4.
- Stevens, C.H., and Stone, P., 2005, Structure and regional significance of the Late Permian(?) Sierra Nevada–Death Valley thrust system, east-central California: *Earth-Science Reviews*, v. 73, p. 103–113.
- Stevens, C.H., Stone, P., and Miller, J.S., 2005, A new reconstruction of the Paleozoic continental margin of southwestern North America: Implications for the nature and timing of continental truncation and the possible role of the Mojave-Sonora megashear, in Anderson, T.H., Nourse, J.A., McKee, J.W., and Steiner, M.B., eds., *The Mojave-Sonora Megashear Hypothesis: Development, Assessment, and Alternatives*: Geological Society of America Special Paper 393, p. 597–618, doi:10.1130/0-8137-2393-0.597.
- Stevens, C.H., Stone, P., Schmitz, M.D., and Paterson, S.R., 2015, Dating of Late Permian deformation in eastern California, in *Proceedings, 2015 Pacific Section American Association of Petroleum Geologists Joint Annual Meeting*, Oxnard, California, 3–5 May, p. 60–61.
- Stewart, J.H., Poole, F.G., and Wilson, R.F., 1972a, Stratigraphy and origin of the Chinle Formation and related Upper Triassic strata in the Colorado Plateau region with a section on sedimentary petrology by R.A. Cadigan and on conglomerate studies by William Thordarson, H.F. Albee, and J.H. Stewart: *U.S. Geological Survey Professional Paper* 690, 336 p.
- Stewart, J.H., Poole, F.G., Wilson, R.F., and Cadigan, R.A., 1972b, Stratigraphy and origin of the Triassic Moenkopi Formation and related strata in the Colorado Plateau region: *U.S. Geological Survey Professional Paper* 691, 195 p.
- Stewart, J.H., Anderson, T.H., Haxel, G.B., Silver, L.T., and Wright, J.E., 1986, Late Triassic paleogeography of the southern Cordillera: The problem of a source for voluminous volcanic detritus in the Chinle Formation of the Colorado Plateau region: *Geology*, v. 14, p. 567–570, doi:10.1130/0091-7613(1986)14<567:LTPOTS>2.0.CO;2.
- Stone, P., and Stevens, C.H., 1988, Pennsylvanian and Early Permian paleogeography of east-central California: Implications for the shape of the continental margin and the timing of continental truncation: *Geology*, v. 16, p. 330–333, doi:10.1130/0091-7613(1988)016<0330:PAEPP>2.3.CO;2.
- Therrien, F., Jones, M.M., Fastovsky, D.E., Herrick, A.S., and Hoke, G.D., 1999, The oldest Triassic strata exposed in Petrified Forest National Park revisited, in Santucci, V.L., and McClelland, L., eds., *National Park Service Paleontological Research, Volume 4: National Park Service Technical Report NPS/NRGRD/GRDTR-99/3*, p. 101–108.
- Torres, R., Ruiz, J., Patchett, P.J., and Grajales, J.M., 1999, Permo-Triassic continental arc in eastern Mexico: Tectonic implications for reconstruction of southern North America, in Bartolini, C., Wilson, J.L., and Lawton, T.F., eds., *Mesozoic Sedimentary and Tectonic History of North-Central Mexico*: Geological Society of America Special Paper 340, p. 191–196, doi:10.1130/0-8137-2340-X.191.
- Tosdal, R.M., 1988, Mesozoic rock units along the Mule Mountains thrust system, southeastern California and southwestern Arizona [Ph.D. thesis]: Santa Barbara, University of California, 365 p.
- Walker, J.D., 1988, Permian and Triassic rocks of the Mojave Desert and their implications for timing and mechanisms of continental truncation: *Tectonics*, v. 7, p. 685–709, doi:10.1029/TC007i003p00685.
- Whitmeyer, S.J., and Karlstrom, K.E., 2007, Tectonic model for the Proterozoic growth of Laurentia: *Geosphere*, v. 3, p. 220–259, doi:10.1130/GES00055.1.
- Wiedenbeck, M., Alle, P., Corfu, F., Griffin, W.L., Meier, M., Oberli, F., von Quadt, A., Roddick, J.C., and Spiegel, W., 1995, Three natural zircon standards for U–Th–Pb, Lu–Hf, trace element and REE analyses: *Geostandards Newsletter*, v. 19, p. 1–23, doi:10.1111/j.1751-908X.1995.tb00147.x.
- Wooden, J.L., Barth, A.P., and Mueller, P.A., 2012, Crustal growth and tectonic evolution of the Mojave crustal province: Insights from hafnium isotope systematics in zircons: *Lithosphere*, v. 5, p. 17–28, doi:10.1130/L218.1.